Simulations of Ground State Fluctuations in Mean-Field Ising Spin Glasses

Stefan Boettcher*
Physics Department, Emory University, Atlanta, Georgia 30322; USA

The scaling of fluctuations in the distribution of ground-state energies or costs with the system size N for Ising spin glasses is considered using an extensive set of simulations with the Extremal Optimization heuristic across a range of different models on sparse and dense graphs. These models exhibit very diverse behaviors, and an asymptotic extrapolation is often complicated by higher-order corrections. The clearest picture, in fact, emerges from the study of graph-bipartitioning, a combinatorial optimization problem closely related to spin glasses. Aside from two-spin interactions with discrete bonds, we also consider problems with Gaussian bonds and three-spin interactions, which behave differently to a significant degree.

I. INTRODUCTION

Ising spin glasses are the paradigmatic model for disorder not only in materials [1], but provide the archetype for complex behavior in many contexts, such as hard combinatorial problems [2, 3], information theory [4], and learning [5, 6]. An Ising spin glass is generally described by the Hamiltonian

$$H \;=\; -\sum_{<i,j>} J_{i,j}\sigma_i\sigma_j \tag{1}$$

with N Ising spins $\sigma_i \in \{\pm 1\}$ and quenched random bonds $J_{i,j}$. The bonds are chosen from a distribution, here, of zero mean and width $\sqrt{\langle J^2\rangle} = J_0$ that is either bimodal ($J_{i,j} \in \{\pm J_0\}$) or Gaussian. The sum parses over all extant bonds $< i, j >$ between any pair of spins σ_i and σ_j. The Sherrington-Kirkpatrick model (SK) [7] is the mean-field limit of Ising spin glasses, in which each spin is coupled to every other spin in the system. To keep the energies E of an equilibrium spin configuration in SK extensive, we set $J_0 = 1/\sqrt{N}$; the other models discussed here are defined on sparse graphs and require $J_0 = 1$.

It is surprising to find still new features of such a well-studied model after some 30 years study. Therefore, the unusual behavior of the distribution of ground-state energies E_0 over the bond disorder in SK has raised significant interest in recent years. This interest is further elevated by its close connection with the statistics of extremely rare events, that in many jammed, disordered systems can become the controlling feature of the dynamics. It was found [8–12] that the fluctuations in E_0 behave in a highly non-normal fashion and rather resemble distributions found in extremal-value statistics [13]. This connection becomes rigorous for the fluctuations of the random-energy model (REM) [14], for which a Gumbel distribution can be derived exactly. The shape in SK shares similarities with a higher-order Gumbel distribution [8, 11, 15] but its precise functional form remains unknown. There exists a high degree of universality in the extreme-value statistics of intrinsically uncorrelated states, but in long-range connected systems with quenched disorder such an assumption may fail. A general discussion of the ordinary versus extreme fluctuations in the SK and other disordered models is provided in Ref. [16].

Of special interest for the energy fluctuations is the variation in width of the distribution with the system size, as it provides important clues to the structural properties of the ground states (or low temperature states generally) [9, 17, 18]. A number of arguments regarding the system-size scaling of the standard deviation for the ground-state energy densities $e_0 = E_0/N$,

$$\begin{aligned}\sigma\left(e_0\right) \;&=\; \sqrt{\langle e_0^2\rangle - \langle e_0\rangle^2} \\ &\sim\; A\,N^{-\rho} + B\,N^{-a} + \ldots \quad (a > \rho)\,,\end{aligned} \tag{2}$$

for $N \to \infty$ have been put forward, leading to values of either [9, 19] $\rho = \frac{3}{4}$ or [20–25] $\rho = \frac{5}{6}$. Both conjectures predict decay that is faster than for normal fluctuations $\rho = \frac{1}{2}$, which would be obtained from the central limit theorem under the assumption of negligible correlations between individual terms of the spin glass Hamiltonian in Eq. (1). While a bound of $\rho \geq \frac{3}{4}$ has been shown [17, 18] for the SK, Gaussian behavior is indeed found for spin glasses on a finite-dimensional lattice [26], and has also been observed on sparse random graphs [9]. Exact values different from any of these are known for the replica symmetric spherical spin glass $\left(\rho = \frac{2}{3}\right)$ and the m-vector spin glass for $m \to \infty$ $\left(\rho = \frac{4}{5}\right)$ [27].

Numerically, both conjectures for ρ on the SK have proven difficult to distinguish with any certainty, and while most initial predictions [8–11] seems to favor a value close to $\rho = \frac{3}{4}$, more recently a trend towards $\rho = \frac{5}{6}$ was found at larger system sizes [12]. That would support the current consensus in the theoretical work [21–23]. Such a larger value is also desirable for consistency between relations connecting ρ to the exponent describing domain wall excitations [19] as found in high dimensions [28].

Here, we report on extensive simulations to clarify this important question regarding the low-temperature properties of spin glasses. The results are at best marginally consistent with any of the theoretical predictions. Since

*Electronic address: www.physics.emory.edu/faculty/boettcher

the data analysis proves to be complicated by transient behavior, we have widened the scope of our investigation to incorporate a large number of related models for comparison. For instance, we provide corresponding data for spin glasses on random regular graphs ("Bethe lattices") of sparse degree, both for two- and three-spin interactions and discrete ($\pm J$) as well as Gaussian bonds. Two-spin coupled spin glasses on Bethe lattices of degree r provide a convenient one-parameter family of models with smoothly extrapolates to SK for increasing degree, $r \to \infty$ [29, 30]. The results are quite similar to those we find in SK, thus, providing a likely trend for the SK behavior itself, but they are equally beset with strong transients. The three-spin data with discrete bonds draws a different picture, consistent with a recent study [31], and also highlights the question of universality of the results when continuous bonds are used. As we have noted before [32], on sparse graphs finite-size corrections may already depend on details of the bond distribution; this dependence appears to extend also to ground-state deviations.

Alternatively, we study the graph bipartitioning problem (GBP) on these Bethe lattices. We find much diminished transients and a consistent extrapolation for the value of ρ. But that value is between – and likely distinct – from $\frac{3}{4}$ and $\frac{5}{6}$. Although it was recently predicted [33] that GBP in the thermodynamic limit is equivalent to the corresponding spin glass at $T = 0$ on those Bethe lattices, it is of course less clear whether such relation would hold at finite size. For instance, finite-size corrections to the average ground state energies already differ significantly between GBP and spin glasses.

This paper is structured as follows: We start with a few remarks about the optimization heuristic used in all of our simulations in Sec. II A. Since the clearest case is provided by GBP, we present our data for this problem first in Sec. III. In Sec. IV, we discuss the SK data at length. In Sec. V, we present the data for the corresponding spin glass problem on Bethe lattices, followed by a similar study on ordinary random graphs in Sec. VI. In Sec. VII, we supplement our investigation with a study of three-spin interactions on a Bethe lattice. We summarize with a few conclusions in Sec. VIII.

II. MEANS AND METHODS

In this section, we introduce the simulation methods and techniques by which the resulting data was analyzed.

A. Optimization Methods

We have employed the Extremal Optimization heuristic (EO) [34–36] in the implementation described previously for the SK spin glass [11] and those on Bethe lattices [30], with various improvements to attain an order of magnitude in speed-up [60]. Resorting to a simple bimodal bond distribution whenever possible allows further an efficient use of integer arithmetic. Not only do discrete bonds provide computational advantages over continuous ones; Gaussian bonds pose significant entropic barriers in addition to the usual complexities faced by local search in a multi-modal energy landscape [37]. To find approximations to GBP ground states, we use EO as described in Ref. [33, 38].

Unlike, for instance, the parallel tempering Monte Carlo technique used at larger system sizes for SK in Ref. [12], which operates at small but finite temperatures, EO generally performs its local search for minima in the landscape formed by the internal energy itself, with activated spin flips as elementary moves [35]. The only free parameter controlling EO was set to $\tau = 1.25$ for discrete problems and somewhat higher at $\tau = 1.5$ for problems with Gaussian weights, and about $0.1\,N^3$ spin flips were executed in each run, restarting form a random initial configuration. At least 2 such restarts were performed for each instance, and the number of runs is doubled on-the-fly whenever a new optimum is found in the latter half of all runs. For some rare instances, more than 10 runs were required, always ensuring that the latter half of all runs merely confirms the previously found optimum but does not exceed it. In each section, we have listed the number of instances treated at each N. Besides trying to reach large sizes, we have often emphasized simulating a very large number of instances on a relatively dense set of intermediate N. We have conducted extensive tests for each model to ensure the accuracy of the results. Testing on testbeds of exactly-solved instance (using branch-and-bound) typically results in perfect agreement, but system sizes are small ($N \approx 50-70$). On larger systems, we have done sample runs with ten-times more updates and found only few inaccuracies, which lead to systematic errors far below statistical errors (unless otherwise noted).

Although all of the problems in this project could be classified as spin glasses, they stand in for a large class of combinatorial problems. It should be noted that the EO heuristic provides data of great detail with only small changes in the implementation. Only the input for the various graph types needed to be changed. (For GBP, we have to impose the additional constraint of vanishing magnetization.) While we treat only mean-field problems here, pertinent results have been obtained previously for structured instances, such as finite-dimensional lattices [39, 40].

B. Data Analysis

To obtain insights into the finite-size scaling of our observables, we study fits of the data generated in our simulations to a number of asymptotic forms. These forms seem to be the most nature candidates to describe corrections to the leading asymptotic behavior. But there can never be an exhaustive list of all possibilities without any theoretical knowledge a-priori. Therefore, we list as

much as possible the data points obtained in the simulations in tables that would allow the readers to pursue their own hypotheses.

Any asymptotic ($N \to \infty$) fit bares considerable risks: Not only may a presumed asymptotic form be insufficient and may, for instance, miss logarithmic corrections, etc. But even if correct, it would certainly fit data for larger system sizes N better than any transients, raising the question of how many data points for lower N to include. Any of these uncertainties can introduce potentially sizable systematic errors, even if the heuristic had been perfectly accurate. Such errors can only be eliminated fully with a theory to compare to, which at present does not exist. The obtained qualities-of-fit Q have to be seen in this context, and a poor Q-value should not be taken immediately as disproving a hypothesis, unless it is seen in relation to alternative fits and a discussion of how much transient data has been included. In fact, to obtain any reasonable Q-values, in each fit we have – somewhat arbitrarily – increased the error bars *uniformly* by a factor of four from the purely statistical errors given as a bracketed uncertainty in the last digit of the simulation data listed in the tables. Such a uniform allowance for systematic errors, either from heuristic inaccuracies or functional uncertainty in the fit, is definitely inadequate and would deserve better consideration in the future.

Thus, we fit the asymptotic extrapolation of the finite-size data towards the thermodynamic limit ($N \to \infty$) for the presumed ground-state energy $\langle e_r \rangle_N$ or cost densities $\langle c_r \rangle_N$ to the following forms, abbreviating $x \in \{c, e\}$:

$$\langle x_r \rangle_N \;\sim\; \langle x_r \rangle_\infty + A\, N^{-\omega} + \dots \tag{3}$$

for just the first-order correction, or

$$\langle x_r \rangle_N \;\sim\; \langle x_r \rangle_\infty + A\, N^{-\omega} + B\, N^{-\omega_1} + \dots \tag{4}$$

as a second order correction, where we have to fix the first-order exponent ω and require $\omega_1 > \omega$ to achieve a stable fit. An alternative second-order, logarithmic fit,

$$\langle x_r \rangle_N \sim \langle x_r \rangle_\infty + A\, N^{-\omega} + B\, \frac{\ln N}{N} + \dots, \tag{5}$$

with arbitrary $\omega < 1$ also seems conceivable.

The asymptotic scaling for the respective deviation exponent ρ proceeds either through a direct fit (to first- or second order) to Eq. (2), or by the corresponding extrapolated form

$$-\frac{\log \sigma}{\log N} \;\sim\; \rho - \frac{\log C}{\log N} + O\left(\frac{N^{-(a-\rho)}}{\log N}\right). \tag{6}$$

Either method has its advantages and disadvantages. A direct fit, plotted on a double-logarithmic scale, provides easier convergence when higher-order terms are included. But the logarithmic scale smoothes out variability or transient in a data set. In turn, the extrapolated form in Eq. (6) is far less forgiving and provides significantly more insight into fluctuations in the data set. When plotted on an $1/\log N$-scale, data that extends over decades is squashed into a relatively small space. But if a solid linear regime emerges, it provides stronger evidence for the existence and value of an exponent than a double-logarithmic plot. The slope of this extrapolation is arbitrary, though, as we could multiply σ by any constant factor without affecting the scaling. We may choose to fix this factor in a way (such as for the spin glasses below) that the $\log C$-term in Eq. (6) vanishes, or (such as for the GBP below) to splay out several plots into one graph. Clearly, such a choice does not alter any linear regime, if it exists. Without such a linear regime, as we will see, it is very difficult to extract satisfactory information from such a fit, even when higher-order (and strongly non-polynomial) corrections are taken into account.

As we have argued in Ref. [32], under certain circumstances it is necessary to consider the cost of frustration (sum of all violated bonds) in a ground state, instead of its energy (difference between all violated and all unviolated bonds). We will switch in our discussion between cost and energy repeatedly. There is a simple linear relation between their average densities,

$$\langle e_0 \rangle_N = 2\, \langle c_0 \rangle_N - \frac{r}{p}\, \langle |J| \rangle_N\,, \tag{7}$$

where r is the (average or fixed) degree and p refers to the number of spins coupled via a single bond. The average absolute bond-weight for the Gaussian distribution of zero mean and standard width ($J_0^2 = 1$ on sparse graphs, $J_0^2 = 1/N$ for SK) is given by $\lim_{N\to\infty} \langle |J| \rangle_N = \sqrt{\frac{2}{\pi}}$, whereas it is simply $\langle |J| \rangle_N = 1$ for a bimodal distribution on a sparse graph. While there is no difference between cost and energy at the level of averages, the corresponding relation of the (co-)variances mixes the fluctuations in cost and energy with that of the absolute bond weights. If in each instance the absolute sum of all bond weights is the same, i. e. a δ-peak without fluctuations, cost and energy fluctuations are proportional. But if the absolute bond weight sum fluctuates (independently) from instance to instance, either energy- or cost-fluctuations will become equally normal-distributed, which leaves at most one of them non-trivial. Typically, for SK cost-fluctuations are trivial (i. e. normal) and energy-fluctuations are interesting, while for sparse graphs with variable degree and/or continuous bonds the role reverses. Only for Bethe lattices (of fixed degree) with bimodal bonds, cost and energy-fluctuations are proportional. When $r \gg 1$ and each spins acquires a nearly extensive number of neighbors, matters get more complicated.

III. GRAPH BI-PARTITIONING ON BETHE LATTICES

In GBP, a graph of (even) N vertices and a certain number of edges is divided into two sets of equal size $N/2$ such that the number of edges connecting both sets, the

Table I: Average cost per spin $\langle c_r \rangle_N$ for approximate ground states of GBP on Bethe lattices of degree $r = 3, \ldots, 10$. The given errors, in parentheses after each average, denote the uncertainty in the last given digit of that average. This uncertainty is solely based on the statistical error. Fits of this data and their plots were discussed previously in Ref. [33] (see Fig. 2 there).

N	$\langle c_3 \rangle_N$	$\langle c_4 \rangle_N$	$\langle c_5 \rangle_N$	$\langle c_6 \rangle_N$	$\langle c_7 \rangle_N$	$\langle c_8 \rangle_N$	$\langle c_9 \rangle_N$	$\langle c_{10} \rangle_N$
32	0.19495(3)	0.35652(4)	0.53893(5)	0.71445(5)	0.91552(6)	1.09781(6)	1.31056(6)	1.49700(7)
40	0.18161(3)	0.34104(3)	0.51730(4)	0.69348(4)	0.88800(5)	1.07190(5)	1.27774(5)	1.46657(6)
50	0.16627(2)	0.32820(3)	0.49487(3)	0.67581(4)	0.85919(4)	1.05003(4)	1.24320(5)	1.44071(5)
64	0.15822(2)	0.31632(2)	0.48312(3)	0.65972(3)	0.84438(3)	1.02997(4)	1.22578(4)	1.41715(4)
80	0.15042(1)	0.30750(2)	0.47119(2)	0.64753(3)	0.82899(3)	1.01495(3)	1.20743(3)	1.39936(3)
100	0.14406(2)	0.30016(2)	0.46138(3)	0.63749(3)	0.81632(3)	1.00232(4)	1.19222(4)	1.38449(4)
128	0.13825(2)	0.29350(1)	0.45240(2)	0.62822(2)	0.80481(3)	0.99082(3)	1.17837(3)	1.37085(3)
160	0.13411(1)	0.28858(2)	0.44582(2)	0.62133(2)	0.79628(2)	0.98220(2)	1.16812(3)	1.36075(3)
200	0.13064(1)	0.28450(1)	0.44037(2)	0.61553(2)	0.78920(2)	0.97498(2)	1.15965(2)	1.35227(3)
256	0.12753(1)	0.28087(1)	0.43545(1)	0.61037(2)	0.78281(2)	0.96852(2)	1.15195(2)	1.34449(2)
320	0.12526(1)	0.27818(1)	0.43185(2)	0.60652(2)	0.77813(2)	0.96370(2)	1.14630(2)	1.33874(3)
512	0.12170(1)	0.27395(1)	0.42607(1)	0.60054(2)	0.77073(2)	0.95605(2)	1.13734(2)	1.32968(2)
1024	0.11852(1)	0.26993(1)	0.42075(1)	0.59497(2)	0.76407(4)	0.94948(4)	1.12965(5)	1.32211(6)
2048	0.11670(4)							

"cutsize", is minimized. The global constraint of an equal division places the GBP among the hardest problems in combinatorial optimization, since determining the *exact* solution with certainty would in general require a computational effort growing faster than any power of N [41]. Applications of graph partitioning reach from the design of integrated circuits (VLSI) [42] to the partitioning of sparse matrices [43], leading to very different requirement regarding the mix of speed and accuracy in a heuristic [44]. In Refs. [45, 46], we have considered a range of different graph ensembles, which can affect characteristics of GBP drastically; here, as in Ref. [33], we merely focus on Bethe lattices, which are locally tree-like such that some analytical results have been derived [47–50]. These Bethe lattices are also known as r-regular graphs, and are generated by fixing the degree r at each vertex, which in turn is connected to other vertices at random.

A. Average Ground State Costs

In Tab. I, we have obtained approximate optima in the cutsize per vertex $\langle c_r \rangle_N$ on Bethe lattices for degrees r between 3 and 10, and graph sizes between $N = 32$ and 2048. Statistical errors of our averages have been kept small by generating a large number of instances for each N and r, typically $n_I \approx 10^6$ for $N \leq 200$, $n_I \approx 10^5$ for $N \geq 256$. Ref. [33] described the implementation of the τ-EO heuristic used to obtain the ground state approximations for GBP. We have presented some of the most salient results of the extrapolation to the thermodynamic limit there.

In Ref. [33], we used a fit with first-order corrections according to Eq. (3) alone, see Tab. 1 and Fig. 2 there. Such a first-order fit to the data from the largest system sizes only is discussed in Tab. II. While the fits produce rather consistent results, with very similar values for ω, there is clearly a distinction between even and odd r in the quality of the fits, indicative of parity effects typical of regular graphs already noted earlier [29, 33].

Table II: Fit of the data in Tab. I to Eq. (3) for the cost c. Only data for $64 < N < 2048$ has been utilized.

r	$\langle c_r \rangle_\infty$	A	ω	ndf	χ^2/ndf	Q
3	0.114765	1.71	0.88	6	0.178	0.98
4	0.265240	1.77	0.85	6	2.124	0.047
5	0.414254	2.35	0.85	6	0.410	0.87
6	0.587974	2.37	0.84	6	0.622	0.71
7	0.755752	3.11	0.86	6	0.138	0.99
8	0.940334	2.93	0.84	6	1.053	0.39
9	1.119390	3.74	0.86	6	0.599	0.73
10	1.310780	3.37	0.83	6	1.836	0.088

Table III: Fit of the data in Tab. I to Eq. (5) with fixed $\omega = \frac{2}{3}$. Only data for $64 < N < 2048$ has been utilized.

r	$\langle c_r \rangle_\infty$	A	B	ndf	χ^2/ndf	Q
3	0.116574	-0.69	-1.29	6	6.347	1.1e-06
4	0.266936	-0.56	-1.28	6	11.886	2.2e-13
5	0.416543	-0.75	-1.73	6	6.770	3.4e-07
6	0.590277	-0.71	-1.75	6	2.311	0.031
7	0.759679	-1.21	-2.45	6	2.585	0.017
8	0.944030	-1.02	-2.29	6	0.645	0.69
9	1.124500	-1.52	-3.01	6	1.747	0.11
10	1.315190	-1.14	-2.66	6	0.600	0.73

A surprising feature of these fits are the values for the finite-size scaling exponent ω. In our previous stud-

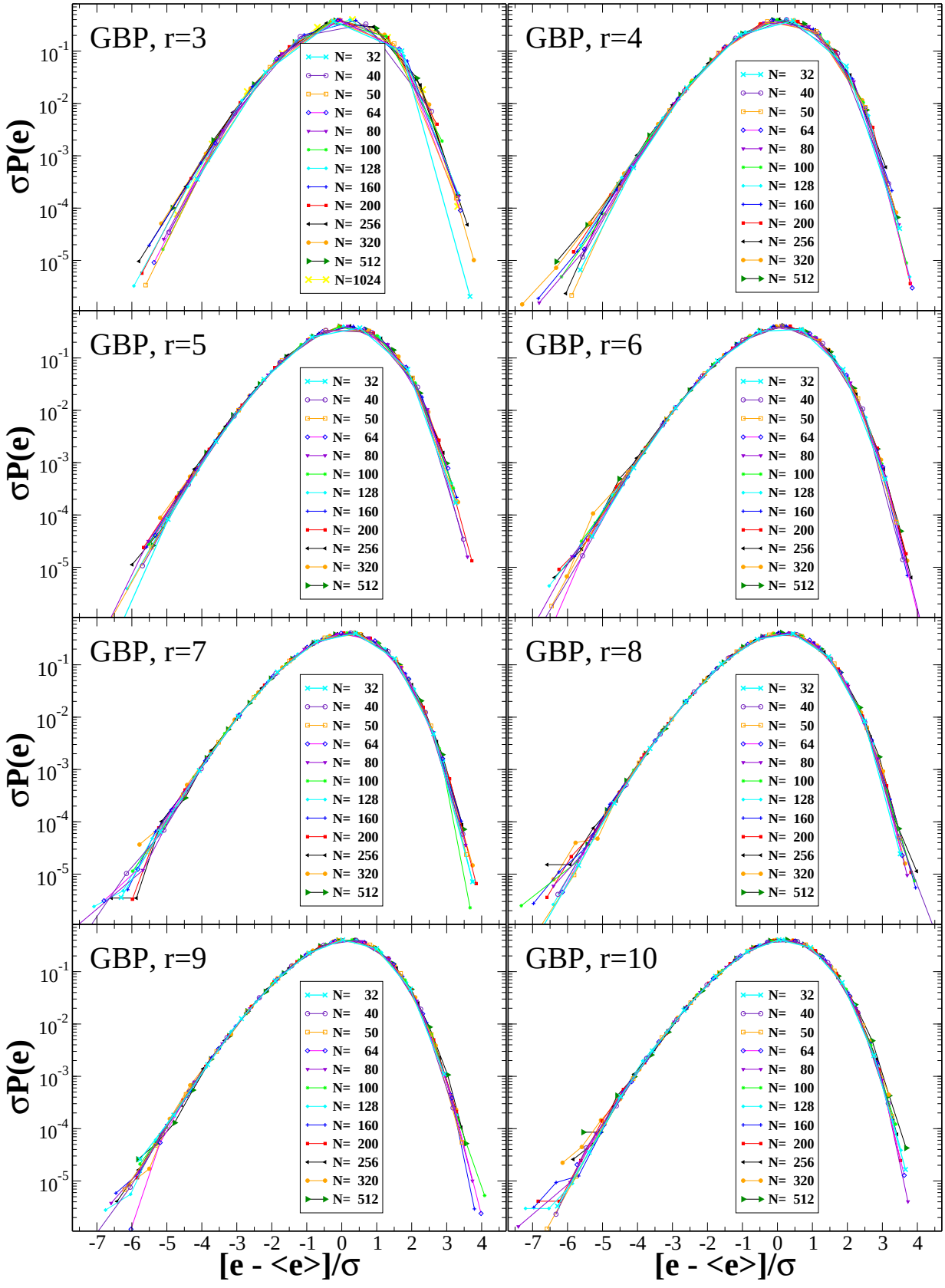

Figure 1: Plot of the PDFs for the ensemble fluctuations of the optimal costs per spin for GBP on Bethe lattices of degree $r = 3, 4, \ldots, 10$. When rescaled by their deviation $\sigma = \sigma\,(c_r)_N$, the data collapses virtually for all system sizes onto a highly skewed master-curve. There appears to be little change in skewness between degrees r.

Table IV: Fit of the data in Tab. I for all N to Eq. (4), but restricting $\omega_1 = 2\omega$.

r	$\langle c_r \rangle_\infty$	A	B	ω	ndf	χ^2/ndf	Q
3	0.114302	1.26	2.53	0.82	9	86.118	0
4	0.265357	1.90	-1.37	0.87	9	1.950	0.041
5	0.413007	1.52	3.62	0.77	9	101.090	0
6	0.588208	2.65	-3.16	0.86	9	0.351	0.96
7	0.753483	1.94	4.31	0.76	9	118.141	0
8	0.940714	3.33	-4.55	0.86	9	0.547	0.84
9	1.116430	2.30	4.90	0.76	9	137.050	0
10	1.311290	3.84	-4.83	0.85	9	0.975	0.46

ies [29, 30] of bimodal spin glasses on Bethe lattices we found throughout that this exponent was most consistent with $\omega = \frac{2}{3}$, which has also been predicted for SK, see Sec. IV A. While it was argued in Ref. [33] that bimodal spin glass and GBP on Bethe lattices should be equivalent in the ground state energy, this equivalence apparently does not extend even to first-order corrections, as the values for ω in these fits are significantly higher. To analyze whether even higher-order corrections could rectify this discrepancy in scaling, we attempt a fit of the form in Eq. (4) with $\omega = \frac{2}{3}$ fixed but variable B and ω_1. Such a fit fails to converge, as in each iteration ω_1 moves closer to ω. Alternatively, we prescribe the form of a plausible logarithmic higher-order correction in Eq. (5). The results of this fit are listed in Tab. III. The quality of the fit is very poor for small degree r but gets progressively better for increasing r, suggesting a possible approach to the SK result for ω for $r \to \infty$. Yet, the results for $\langle c_r \rangle_\infty$ are somewhat less in agreement with the conjectured equivalence in Ref. [33]. Generally, if the next-order correction contains a (possibly polynomial) logarithmic dependence of this sort, any attempt to predict ω may be futile.

Another alternative form to fit is provided by a series expansion in powers of $N^{-\omega}$. Thus, fitting to Eq. (4) with $\omega_1 = 2\omega$ we obtain the results listed in Tab. IV. Now, the results for $\langle c_r \rangle_\infty$ are again in good agreement with the conjecture but the quality of the fit is not improved over the mere first-order fit in Tab. II. Interestingly, this form is now a better fit with *even* values for r but terrible for odd ones, reversing the trend from the previous fits. Correction terms may differ between even and odd r not only in their constants but in their very form.

B. Ground State Fluctuations

In Fig. 1, we plot the probability density functions (PDF) of ground-state costs over the ensembles of Bethe lattices. Unlike for the spin glass problems below, transients due to finite-size effects diminish quickly. This leads to a solid collapse of the data when properly rescaled by their deviations $\sigma(c_r)_N$ in Eq. (2), apparently with little difference in the scaling function even for varying degrees r.

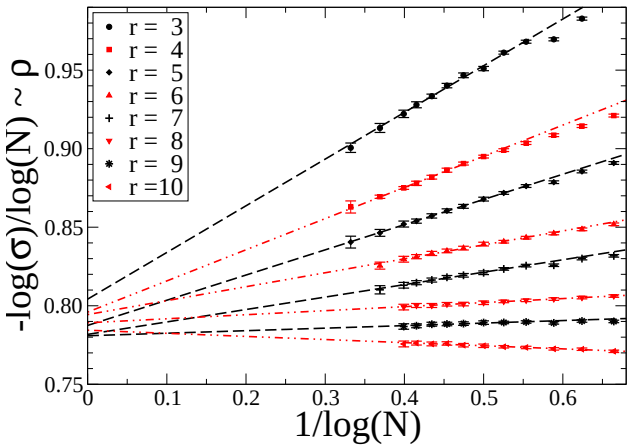

Figure 2: Extrapolation in the limit $N \to \infty$ for the exponent ρ, defined in Eq. (2), from the deviations $\sigma(c_r)_N$ in Tab. V obtained from the distribution of GBP ground state. Appropriately rescaled via Eq. (6), the data for each degree r extrapolates linearly to the thermodynamic limit, with rapidly diminishing transients. Note that for each r the fitted region spans at least one decade in system size N. The goodness-of-fit is $Q = 1$ for all r except for $r = 3$, where $Q \approx 0.73$.

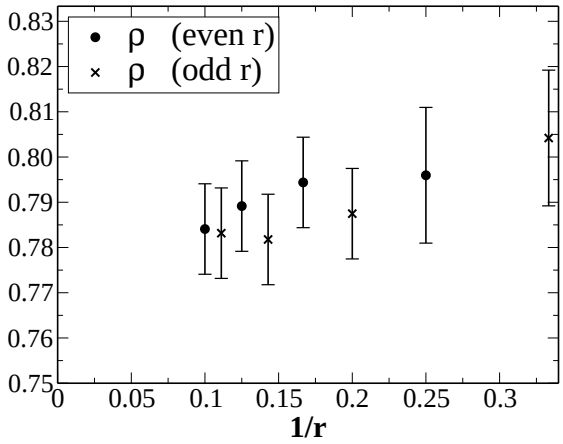

Figure 3: Extrapolated values of ρ for each degree r, obtained from Fig. 2, plotted as a function of inverse degree. For even and odd values of r separately, each sequence extrapolates to value of $\rho_\infty = 0.77(2)$ for $r \to \infty$. The error bars result from the fits in Fig. 2; systematic errors, e. g. due to higher-order corrections ignored in those fits, are potentially larger.

In Tab. V, we list the deviations $\sigma(c_r)_N$, as defined in Eq. (2), for each degree r and system size N. A closer look at these deviations indeed provides a robust extrapolation for the exponent ρ. Eq. (6 should yield a linear extrapolation for the exponent ρ when plotted vs. $1/\log N$, assuming negligible corrections (i. e. $N^{-a} \ll N^{-\rho}$). In Fig. 2, we show these plots for all values of r. It is apparent that transient behavior decays very quickly, and a

Table V: Standard deviation of the ground-state costs in GBP. Statistical errors are estimated as $\sigma/\sqrt{n_I}$, where n_I refers to the number of instances considered. Appropriately rescaled, this data is plotted also in Fig. 2. (Some of the data, in particular, for larger N and r, shows an obvious systematic bias due to two likely sources: a bad approximation for some ground states and an undercount of rare instances with costs extremely far from the average. These data points have been left out of Fig. 2.)

N	$\sigma(c_3)_N$	$\sigma(c_4)_N$	$\sigma(c_5)_N$	$\sigma(c_6)_N$	$\sigma(c_7)_N$	$\sigma(c_8)_N$	$\sigma(c_9)_N$	$\sigma(c_{10})_N$
32	0.03206(3)	0.04108(4)	0.04561(5)	0.05222(5)	0.05598(6)	0.06118(6)	0.06470(6)	0.06910(7)
40	0.02664(3)	0.03428(3)	0.03814(4)	0.04370(4)	0.04680(5)	0.05129(5)	0.05419(5)	0.05790(6)
50	0.02252(2)	0.02860(3)	0.03215(3)	0.03653(4)	0.03953(4)	0.04301(4)	0.04564(5)	0.04869(5)
64	0.01784(2)	0.02333(2)	0.02615(3)	0.02998(3)	0.03228(3)	0.03539(4)	0.03747(4)	0.04009(4)
80	0.01482(1)	0.01945(2)	0.02192(2)	0.02511(3)	0.02710(3)	0.02967(3)	0.03146(3)	0.03367(3)
100	0.01253(2)	0.01622(2)	0.01837(3)	0.02096(3)	0.02280(3)	0.02490(4)	0.02639(4)	0.02825(4)
128	0.01012(2)	0.01329(1)	0.01517(2)	0.01725(2)	0.01877(3)	0.02051(3)	0.02179(3)	0.02329(3)
160	0.00847(1)	0.01113(2)	0.01269(2)	0.01445(2)	0.01573(2)	0.01716(2)	0.01829(3)	0.01948(3)
200	0.00712(1)	0.00935(1)	0.01066(2)	0.01209(2)	0.01323(2)	0.01442(2)	0.01536(2)	0.01641(3)
256	0.00582(1)	0.00769(1)	0.00878(1)	0.00996(2)	0.01092(2)	0.01183(2)	0.01271(2)	0.01351(2)
320	0.00490(1)	0.00643(1)	0.00734(2)	0.00835(2)	0.00919(2)	0.00995(2)	0.01069(2)	0.01140(3)
512	0.00336(1)	0.00441(1)	0.00509(1)	0.00580(2)	0.00638(2)	0.00697(2)	0.00746(2)	0.00798(2)
1024	0.00195(1)	0.00253(1)	0.00295(1)	0.00339(2)	0.00386(4)	0.00428(4)	0.00463(5)	0.00506(6)

smooth linear extrapolation is obtained. Also re-assuring is the fact that this data shows a small even/odd effect, just as for the costs above in Sec. III A. The sequence of extrapolants for ρ appear to converge towards the same value of $\rho = 0.77(2)$, at least for $r \to \infty$. It is surprising to find such an apparently non-trivial result in such a simple mean-field model. Comparing with theory, it comes closest to the value of $\rho = \frac{3}{4}$ previously proposed in Ref. [9] and seems far from that proposed for the SK model, $\rho = \frac{5}{6}$ [22–25]. There is, of course, no reason for it to be equal to that of SK. But the in-between value found here for GBP is arguably close to the corresponding extrapolations for the spin glasses below, which by themselves remain inconclusive due to strong transients up to large system sizes.

IV. SHERRINGTON-KIRKPATRICK MODEL

We reconsider finite-size corrections in the SK model by expanding on the simulations in Ref. [11] with substantially more instances at many more system sizes, see Tab. VI. It is found that the corrections to the average energies permit fits of reasonable quality with systematic improvements when higher-order corrections are incorporated, but the discussion of the energy fluctuations remains largely inconclusive. Interestingly, this scenario is the converse of that found in Sec. III for GBP.

A. Average Ground State Energy

First, we want to consider the average energies, which provide an assessment of the quality of our simulations in reference to exactly known results about SK; a necessary step preliminary to a more demanding analysis of the data. In Fig. 5, we plot the data for the average ground-state energy density $\langle e_0 \rangle_N$ from Tab. VI for the different N. It has been argued on the basis of theoretical studies [52, 53] at or near T_c and on previous numerical investigations [11, 12, 21, 29, 54], that finite-size corrections to the energy behave for all $T \leq T_c$ according to Eq. (3) with $\omega = \frac{2}{3}$. We find this expectation confirmed within numerical accuracy, see Fig. 4 (left). Fig. 4 also shows that a higher-order correction according to Eq. (4) even improve on this leading behavior substantially, which is plotted as fit to the data in Fig. 5.

Table VI: List of all the data obtained with EO in sequence of system size N. Given are the number of instances n_I considered at each N, and the average ground-state energy density $\langle e_0 \rangle_N$ and average standard deviation $\sigma(e_0)$ over these instances.

N	n_I	$\langle e_0 \rangle_N$	$\sigma\,(e_0)$	N	n_I	$\langle e_0 \rangle_N$	$\sigma\,(e_0)$
15	5000000	-0.64449(3)	0.0670	127	732463	-0.73538(2)	0.0147
17	5000000	-0.65441(3)	0.0614	149	723526	-0.73828(2)	0.0130
21	5000000	-0.66931(2)	0.0531	169	624094	-0.74029(2)	0.0119
25	5000000	-0.67994(2)	0.0471	199	351317	-0.74273(2)	0.0104
31	1480000	-0.69127(3)	0.0407	225	329043	-0.74424(2)	0.0095
35	5000000	-0.69701(2)	0.0374	255	255572	-0.74587(2)	0.0086
41	5000000	-0.70371(2)	0.0335	299	454555	-0.74759(1)	0.0077
49	5500000	-0.71049(1)	0.0295	349	317264	-0.74910(1)	0.0068
55	5000000	-0.71442(1)	0.0272	399	204045	-0.75030(1)	0.0061
63	5000000	-0.71872(1)	0.0246	511	51246	-0.75233(2)	0.0050
69	1000000	-0.72113(2)	0.0232	549	144912	-0.75278(1)	0.0048
79	5000000	-0.72505(1)	0.0208	649	59717	-0.75383(2)	0.0042
89	1000000	-0.72783(2)	0.0192	799	25257	-0.75491(2)	0.0037
99	800000	-0.73043(2)	0.0177	1023	5338	-0.75615(4)	0.0031
109	816132	-0.73242(2)	0.0165	2047	403	-0.7583(1)	0.0020

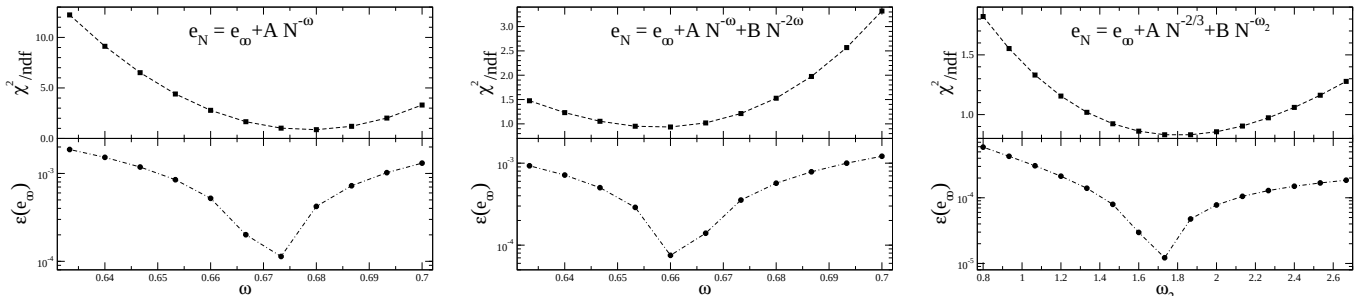

Figure 4: Various fits to the average ground state energies $\langle e_0 \rangle_N$ of SK in Tab. VI. Left-most, we consider first-order corrections only for a fit involving the thermodynamic limit-value e_∞ and the correction amplitude A for varying the correction exponent ω. The best-quality fit to this form, possessing minimal χ^2/ndf, occurs just above $\frac{2}{3}$ at $\omega \approx 0.68$. Adding a higher-order correction (with coefficient B, middle panel), a square of the first-order term, bottoms out at $\omega \approx 0.66$ with much lower χ^2/ndf values overall. Instead, fixing the first-order exponent to $\omega = \frac{2}{3}$ and varying the second-order exponent ω_1 (right panel) implicates an optimal exponent much above 2ω, namely $\omega_1 \approx 1.8$. Remarkably, the optimal choice for ω or ω_1 about coincides in all three fits with the lowest relative error $\epsilon\,(e_\infty)$ (lower panels) in the fitted value for e_∞.

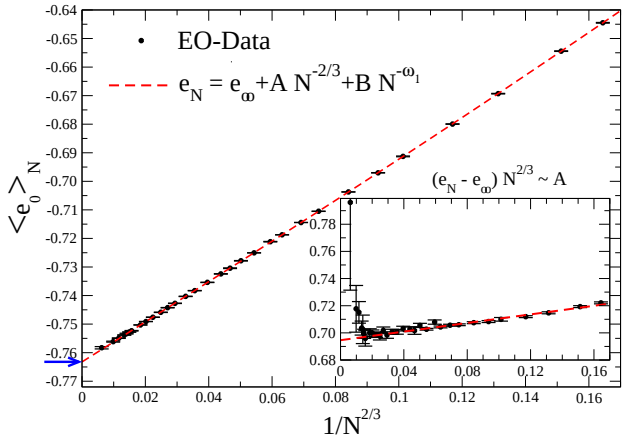

Figure 5: Extrapolation plot of the average ground-state energy densities $\langle e_0 \rangle_N$ from Tab. VI as a function of the presumed finite-size corrections, $1/N^{\frac{2}{3}}$. The statistical errors indicated are much smaller than symbol sizes. For $N \to \infty$, the EO-data extrapolates to the Parisi energy [51], $\langle e_0 \rangle_\infty = -0.7631667265(6)$, at the intercept. The indicated fit (dashed line) predicts $e_\infty = -0.76323(5)$. The slope of the line is $A = 0.70(1)$, consistent with the inset, which shows the same data appropriately rescaled to extrapolate for A. It is $B \approx 0.48$, and $\omega_1 \approx 1.8$ suggests surprisingly weak higher-order corrections, see also Fig. 4.

We can obtain a revealing insight into the quality of the EO-data by extracting the leading behavior to explore the correction term in more detail. Because the energy in the thermodynamic limit is well-known [51], $\langle e_0 \rangle_\infty = -0.7631667265(6)$, we can rewrite Eq. (3) as

$$A \;\sim\; [\langle e_0 \rangle_N - \langle e_0 \rangle_\infty]\, N^{\frac{2}{3}} + \ldots \qquad (N \to \infty), \quad (8)$$

and plot the EO-data in this form in the inset of Fig. 5. Since the form of higher-order corrections are unknown, we plot the data again as a function of $1/N^{\frac{2}{3}}$, which provides a near-linear collapse of the data and an extrapolated value for the amplitude $A \approx 0.695(5)$, which is consistent with the value obtained by the fit in Fig. 5. But the most important aspect of the inset resides in the sharp crossover in the behavior of the data at around $N \approx 1000$. The consistent behavior of the data for $N \lesssim 1000$ suggest sufficient numerical accuracy in the obtained ground state energies to this level of analysis, without any discernible systematic bias. The data points for $N = 799$ and 1024 both exhibit a systematic error of about $\Delta A/A \approx 2/70 \approx 3\%$ in the prediction of A, hence, a relative systematic error of $\epsilon\,(e_\infty) = \Delta e_\infty/e_\infty \sim \Delta A/N^{2/3}/e_\infty \approx 0.03\%$ (see also Fig. 4) in the prediction of typical ground state energies overall. Unfortunately, the systematic error for the $N = 2047$ data point is about $\Delta A/A \approx 1/7 \approx 15\%$, leading to a relative systematic error of 0.1% in the prediction of putative ground states, which is sufficiently noticeable in Fig. 5 to exclude that point from the extrapolation.

It is worthwhile to compare the inset of Fig. 5 with the corresponding plot, the inset of Fig. 1, in Ref. [12]. While the data there is also falling for increasing N [arguably to the same asymptotic value of $A \approx 0.7$, see Eq. (8)], the variation of the data there is far more rapid. Point for point, the data there represents a systematically higher value in the average ground-state energy than is obtained here. This could potentially indicate a bias in the heuristic methods used, which may fail to find true ground states across the board. (Notably, the data there does not show drastic degradation in the quality of the results for increasing N as is found here.) Alternatively, such disagreement could be attributed to the difference in the bond distribution used: Gaussian there and bimodal here. Although the leading thermodynamic properties should be universal, higher-order corrections can be sensitive to microscopic details.

In Fig. 4, we present an alternative procedure to explore corrections that also allows a probe of higher-order terms. In this procedure, we select (the most important) one of the parameters to be fitted as fixed and evaluate the quality of the fit for the remaining parameters over a

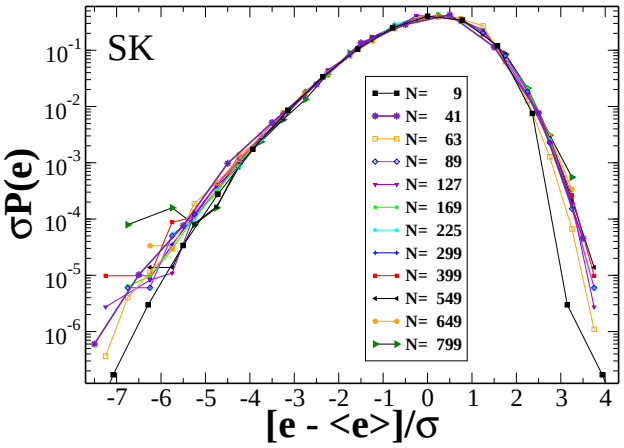

Figure 6: Plot of the probability density functions (PDF) of obtained ground-state energy densities e_0 for SK in units of the standard deviation σ. For reference, the *exact* probabilities for $N = 9$ are re-plotted from Ref. [55]. Unlike for the PDFs for GBP in Fig. 1, there is a significant finite-size effect noticeable especially in the right tail of the distribution.

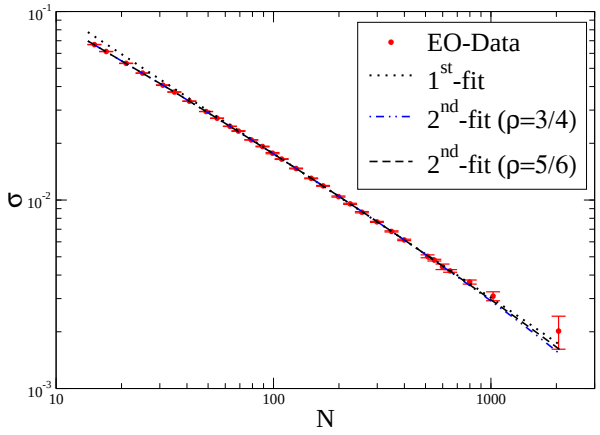

Figure 7: Double-logarithmic plot of the data from Tab. VI for $\sigma_N\,(e_0)$ as a function of N. The data is fitted by a first-order fit with $a + bN^{-\rho}$ restricted to $100 < N < 800$ (dotted line), giving $\rho \approx 0.76$ with a $\chi^2/ndf \approx 0.24$ for $ndf = 13$. Second-order fits with $a + bN^{-\rho} + cN^{-a}$ allowing all $N < 800$ and fixed $\rho = \frac{3}{4}$ (dash-dotted line) or $\rho = \frac{5}{6}$ (dashed line) both give essentially indistinguishable results with a $\chi^2/ndf \approx 0.7$ for $ndf = 25$ in either case. For $\rho = \frac{3}{4}$ we find $a \approx 1.3$, and for $\rho = \frac{5}{6}$ it is quite consistent with unity, $a \approx 1$.

range of values for the selected one. As a measure of quality, we utilize χ^2 per numbers of degree of freedom (ndf), which should be minimized. The first panel displays this procedure for just the first-order correction, again confirming the expectation of Eq. (3). In the remaining two panels we test possible higher-order corrections. In the first of these, we test a fit to a regular Taylor series in powers of $N^{-\omega}$ to second order. Incorporation of such a second-order term improves the quality of the fit noticeably over the first-order term alone. Furthermore, the optimal choice for ω again proves consistent with $\frac{2}{3}$,

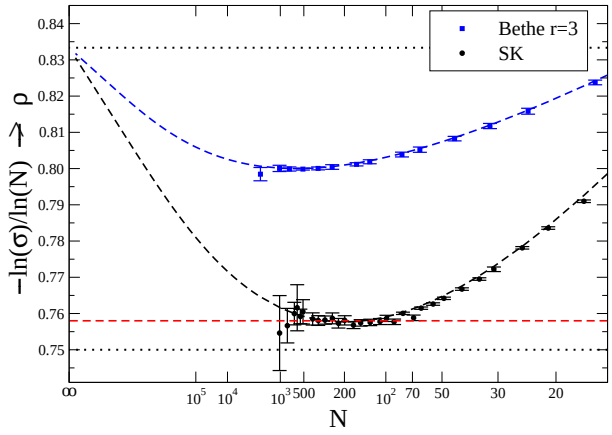

Figure 8: Extrapolation plot according to Eq. (6) towards a prediction of ρ at the ordinate-intercept for SK (black circles) and spin glasses on Bethe lattices (blue squares). The abscissa denotes the system sizes N on a scale of $1/\log N$. A linear fit (red-dashed line) of the SK data in the apparent scaling regime for $N \geq 80$ predicts a value of $\rho \approx 0.76$. The inclusion of the alternative value $\rho = \frac{5}{6}$ (dotted line) here shows the dramatic change required for the data to attain such a value. Yet, a fit (black-dashed line) according to Eq. (6) involving non-linear corrections down to the smallest N is possible, if $\rho = \frac{5}{6}$ is assumed. The corresponding situation for Bethe lattices makes such an extrapolation further plausible.

despite the extra degree of freedom provided, which attests to its robustness. Then, taking $\omega = \frac{2}{3}$ as a given, we explore an independent second-order correction with scaling exponent ω_1. This yields the highest-quality fit thus far, also used in Fig. 5, but predicts that ω_1 would be much larger than simply 2ω, suggesting that such corrections would be even weaker.

We have also tried to fit higher-order corrections of the form $1/N$ or $\ln N/N$ in addition to $1/N^{\frac{2}{3}}$ corrections, which are plausible by analogy with the results obtained for finite-size corrections near the critical temperature [52, 53]. A fit to Eq. (5) does not produce acceptable results compared to those found in Fig. 4 for any value of ω. Instead, a fit to Eq. (4) with $\omega_1 = 1$ fixed produces a very narrow window of reasonable results near $\omega = \frac{2}{3}$ but at best of the quality of what is seen correspondingly at $\omega_1 = 1$ in the last panel of Fig. 4. Further higher-order corrections may improve on this alternative. But if the ratio between a previous and its next higher-order correction is a weakly falling function, i. e. $(1/N)\,/\left(1/N^{\frac{2}{3}}\right) = N^{-\frac{1}{3}} \approx 0.1$ at least for $N \approx 1000$ here, resolving the impact of such corrections with the available data becomes near impossible and they can never be fully excluded.

B. Ground State Energy Fluctuations

Next, we consider the distribution of ground state energies around their averages. In units of their standard de-

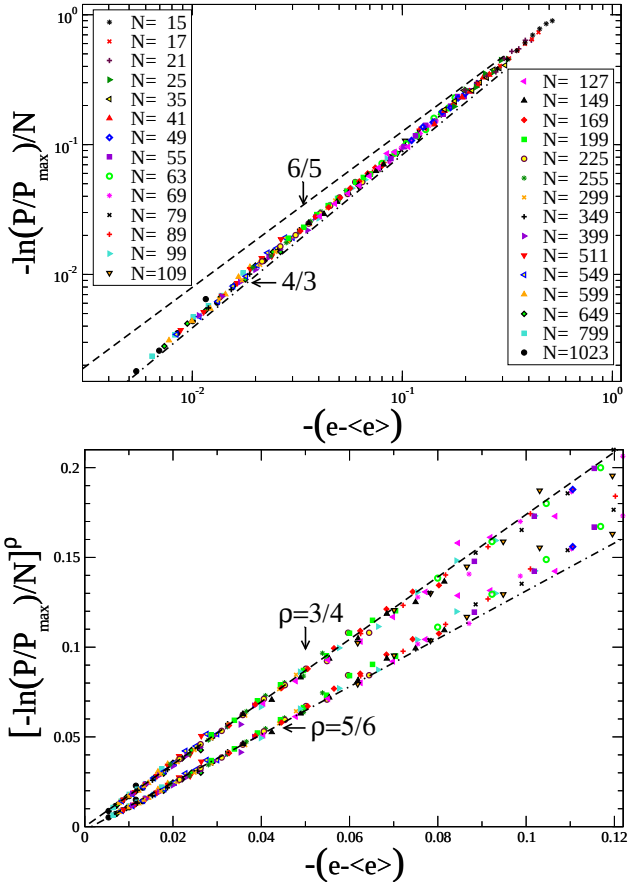

Figure 9: Data collapse on logarithmic scale of all SK data for energies *smaller* than the average from Fig. 6. On top, rescaled by an appropriately chosen $P_{\max}$, the data collapses onto a power-law curve, which exhibits scaling over more than a decade. (Transient data points with P too close to $P_{\max}$ have been removed for clarity.) The collapse is most consistent (see dash-dotted line) with $\rho^{-1} = \frac{4}{3}$ and differs, although only slightly, from $\rho^{-1} = \frac{6}{5}$ (dashed line). On the bottom, the same data (for $N > 100$) is plotted on a linear scale. In this form, $\rho = \frac{3}{4}$ is clearly more consistent with linear scaling (dashed straight lines guide the eye).

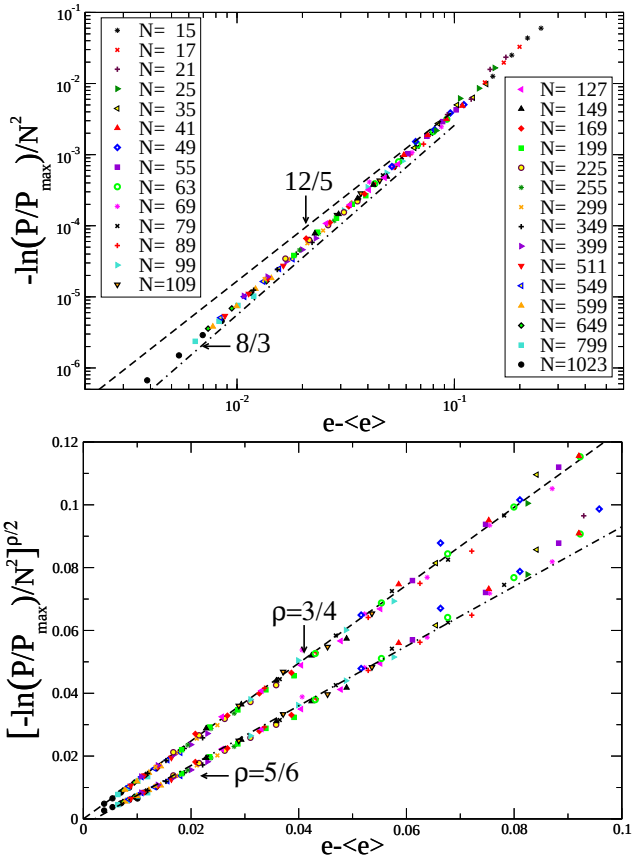

Figure 10: Data collapse on logarithmic scale of all SK data for energies *larger* than the average from Fig. 6. Rescaled by an appropriately chosen $P_{\max}$, the data collapses onto a power-law curve, which exhibits scaling over more than a decade. (Transient data points with P too close to $P_{\max}$ have been removed for clarity.) The collapse is most consistent (see dash-dotted line) with $\rho^{-2} = \frac{8}{3}$ and differs, again only slightly, from $\rho^{-2} = \frac{12}{5}$ (dashed line). On the right, the same data (for $N > 50$) is plotted on a linear scale. In this form, $\rho = \frac{3}{4}$ is clearly more consistent with linear scaling (dashed straight lines guide the eye).

viation, the probability density function (PDF) for each value of N exhibits clearly the asymmetric shape that is skewed towards a broader (exponential) tail of instances with lower than average ground state energy and a cut-off that is much sharper than exponential for those with higher energy. This shape is largely unchanged across the sizes and can be shown, by *exhaustive* enumeration [55] of the *entire* ensemble for $N \leq 9$, to arise already for very small N. In Fig. 6 we show the PDF for all system sizes, which demonstrates the skewness and the small variation of the shape with N. Yet, finite size effects larger than for GBP in Fig. 1 emerge deep in the tails of these PDFs.

Unlike the overall shape of the PDF for energy fluctuations, their actual width, measured in terms of the standard deviation $\sigma_N(e_0)$ in Eq. (2), varies in a characteristic way with N. A plot of the data for $\sigma_N(e_0)$ in Tab. VI on a double-logarithmic scale in Fig. 7 suggests a power-law decay with N, but the data does not exhibit purely linear behavior on this scale, as a simple fit reveals. Only when we restrict to $N > 100$, a fit of the data according to Eq. (2) with just the leading (ρ-dependent) term provides satisfactory results, with a value of ρ just above $\frac{3}{4}$. A more consistent fit of all the data is provided when higher-order corrections are considered. This can only succeed for a reasonable, fixed value of ρ, we indeed accomplish almost identical fits of this sort for either $\rho = \frac{3}{4}$ or $\rho = \frac{5}{6}$ (and probably any nearby value), see Fig. 7. In this regard, the fit for fixed $\rho = \frac{5}{6}$ has the added benefit that the higher-order term appears to scale with $a \approx 1$, a likely candidate for a next-order correction. But if leading and next-order correction are that close, for instance $N^{-\frac{5}{6}}/N^{-1} \sim N^{\frac{1}{6}}$, to obtain the asymptotic scaling of ρ separated by a decade from any transient behavior would

require results for $N \gtrsim 10^6$. Thus, with the present data, a conspiracy between such terms leading to the observed behavior could not be excluded.

To illustrate the difficulty more clearly, we follow the procedure for GBP in Sec. 2 and extrapolate for ρ according to Eq. (6). The variables $y = -\log\sigma/\log N$ plotted vs $x = 1/\log N \to 0$ should provide an asymptotically linear extrapolation (with exponentially small corrections $\sim xe^{-(a-\rho)/x}$, if $a > \rho$) towards the exponent ρ at the y-intercept for $N \to \infty$. Plotting the SK data up to $N \approx 1000$ in this fashion in Fig. 8 again indicates a value just above $\rho = \frac{3}{4}$ and apparently far below $\rho = \frac{5}{6}$. But unlike the GBP data in Fig. 2, the data for SK has still transient features even for such large values of N. Only a non-linear fit according to all three terms in Eq. (6), but taking an already *fixed* $\rho = \frac{5}{6}$ as given, makes such a high value for ρ plausible. Further support for such a higher value of ρ is provided by the following study of spin glasses on Bethe lattices. On the other hand, the GBP example above and the result for the m-vector model of $\rho = \frac{4}{5}$ [27] would suggest that an altogether different value of ρ between these two rational values is conceivable. In fact, a purely linear extrapolation in Fig. 8 and the fit in Fig. 7 for $N \gtrapprox 100$ would lead to an asymptotic value for ρ very close to that of GBP in Sec. III above.

C. Extreme Fluctuations

Considering the large amount of data we have obtained for SK, we can inspect further details of the energy fluctuations. In particular, we can look deeper into the tails of the PDFs displayed in Fig. 6, where they are rescaled by their respective σ_N. Here, we treat these PDFs unrescaled, according to the form proposed in Ref. [24], suggested by the spherical spin glass [56]. In Ref. [24], it was argued that for ground state energies lower than the average, the corresponding branch far in the negative tail of each PDF falls exponentially with an argument proportional in N, while configurations with larger energies are particularly rare for larger system sizes such that the positive tail is suppressed by a factor N^2. This system-size dependence is largely lost when each PDF is rescaled by its width σ_N in Fig. 6.

In Figs. 9 and 10, we extract the argument of the exponential tails and plot the data for each tail reduced by the indicated power of N. In the process, the PDF-data $P(e)$ for each system size has to be gauged by an arbitrary reference point $P_{\max}$ and transient behavior too close to the average or statistically deficient data too deep in the tails has to be discarded. The resulting collapse of all the intermediate data onto a power-law function is presented in the upper panel of each figure on a logarithmic scale. According to Ref. [24], the power-law exponent can be interpreted as ρ^{-1} for $e \ll \langle e\rangle$ and as ρ^{-2} for $e \gg \langle e\rangle$. To provide a reference, we have include lines corresponding to $\rho = \frac{3}{4}$ and $\rho = \frac{5}{6}$ in these plots. While the differences are again slim (and it could be argued that true asymptotic behavior has not been reached), the consistent scaling collapse of this vast amount of data seems to favor a value closer to $\rho = \frac{3}{4}$ again. Furthermore, both tails independently exhibit similar scaling behavior.

When viewed on a linear scale, by taking the respective power, only a value closer to $\rho = \frac{3}{4}$ provides consistent linear behavior for the extant data (see the lower panel of Figs. 9 and 10). In Ref. [24], a similar linear plot was provided (for the positive branch only) in which the largest system size considered there, $N = 150$, was judged consistent with $\rho = \frac{5}{6}$. It is clear from our direct comparison here, that even with the vast amount of additional data an ultimately conclusive decision on the true value of ρ is elusive here. The comparison also shows that an analysis of these tails on a logarithmic scale is favorable over a linear scale which squashes the most interesting data points for larger system sizes. Even on a logarithmic scale, though, it is not easy to extract the relevant asymptotic information as ever deeper in the tails, only ever smaller-sized systems contribute. But overall, in this data, small-sized and large-sized systems seem to follow similar scaling and project a self-consistent picture.

V. SPIN GLASSES ON BETHE LATTICES

To provide a new perspective on the ground-state energy fluctuations in SK, we revisit spin glasses with $\pm J$-bonds on Bethe lattices (SG), in particular, on those of degree $r = 3$. A similar study has been undertaken in Ref. [29, 30], which concerned thermodynamic averages of ground state energies and entropies. Here, we extend the sampling of ground state energies to measure the PDF of ground state energy fluctuations and the scaling of their width. To that end, in Tab. VII we have added a large number of instances at each system size, up to $N = 4096$. Unlike for Bethe lattices of higher degree, at degree three we can utilize exact methods [39, 40, 57] to reduce the number of variables in the optimization problem by about 42%, hence, making larger system sizes accessible at sufficient statistics.

A. Average Ground State Energy

In Fig. 11, we present the average energy densities obtained with EO at the system sizes simulated. As in Ref. [29], the extrapolation of the data is virtually linear when plotted as function of $N^{-\frac{2}{3}}$. Such a linear extrapolation yields $\langle e_3\rangle_\infty = -1.2715(1)$ for the thermodynamic energy density, consistent with the value determined in Ref. [29] and consistent with the one-step replica-symmetry breaking result reported in Refs. [3, 58]. Remarkably, an attempt at adding a higher-order correction term contrasts with the same discussion for SK. Neither of the two types of higher-order fits presented in Fig. 4 provide reasonable results here. In turn, a fit to

Table VII: List of all the data obtained with EO for Bethe lattices of degree $r = 3$ for various system sizes N. Given are the number of instances n_I considered at each N, and the average ground-state energy density $\langle e_0 \rangle_N$ and standard deviation $\sigma(e_0)$ over these instances.

N	n_I	$\langle e_0 \rangle_N$	$\sigma(e_0)$
16	1000000	-1.1467(1)	0.10177
32	1000000	-1.19375(6)	0.06003
44	1680320	-1.20895(4)	0.04695
64	1000000	-1.22314(4)	0.03515
80	1486688	-1.23005(2)	0.02952
128	2000000	-1.24153(1)	0.02043
160	3273585	-1.24583(1)	0.01714
256	1498807	-1.25296(1)	0.01181
350	4015909	-1.25660(1)	0.00921
512	7638942	-1.26007(1)	0.00680
750	1718511	-1.26274(1)	0.00501
1024	743404	-1.26444(1)	0.00390
2048	113389	-1.26710(1)	0.00226

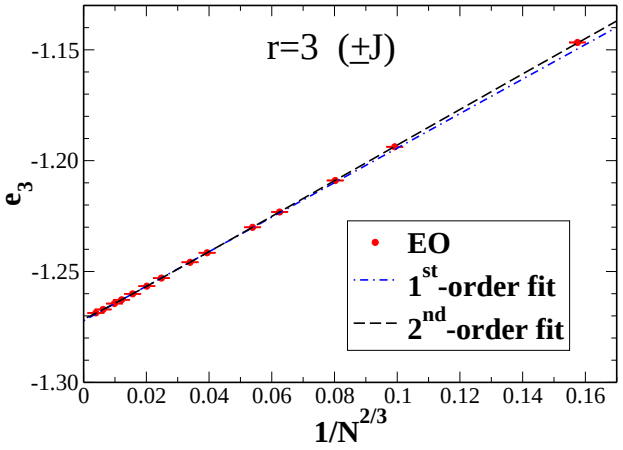

Figure 11: Extrapolation plot of the average ground-state energy densities $\langle e_0 \rangle_N$ for Bethe lattices of degree $r = 3$ as a function of the presumed finite-size corrections, $1/N^{\frac{2}{3}}$. As in Fig. 5, the statistical errors indicated are much smaller than symbol sizes. For $N \to \infty$, irrespective of the order of the fit, the data extrapolates to $\langle e_0 \rangle_\infty = -1.2715(1)$ at the intercept.

Eq. (5), which failed for SK, does converge on this data, see Fig. 12. Across the plotted regime, the thermodynamic value for e_∞ remains quite robust. The optimum is rather close to $\omega = \frac{2}{3}$; such a $2nd$-order fit including ω also shown in Fig. 11 converges to $\omega \approx 0.677$.

B. Ground State Energy Fluctuations

In Fig. 13, we show the probability density functions (PDF) of the energy densities around those averages. Overall, those PDFs are a bit more symmetrical than for SK in Fig. 6, but exhibit even more finite-size effects

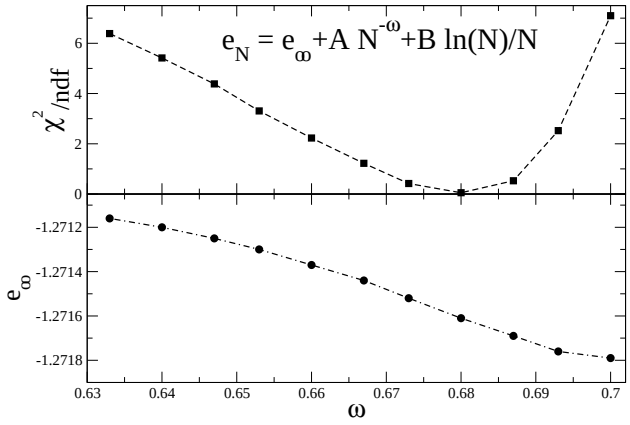

Figure 12: Second-order fit over a range of fixed ω, with logarithmic corrections, to the average ground state energies $\langle e_0 \rangle_N$ for spin glasses on Bethe lattices of degree $r = 3$ in Tab. VII.

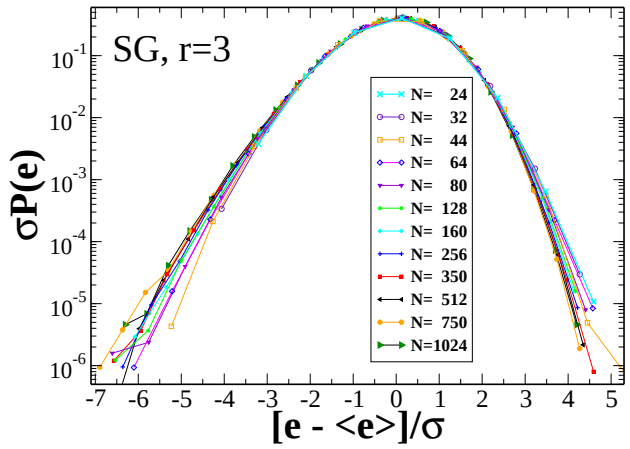

Figure 13: Plot of the probability density functions (PDF) of obtained ground-state energy densities e_0 for the spin glass on a Bethe lattice of degree $r = 3$ in units of the standard deviation σ. Here, in comparison with Figs. 1 and 6, significant finite-size effects are detectable in both tails.

in both tails, especially in comparison with the corresponding PDFs of GBP in Fig. 1. Despite their more symmetrical appearance, the scaling with N of the deviations σ listed in Tab. VII seems to indicate an even higher value of ρ, as Fig. 8 suggests. There, those σ for the Bethe lattice are displayed in an extrapolation plot together with that of SK, to highlight their similarity. This data is somewhat smoother than for SK, but just as much beset with transients. A family of extrapolants for each degree r seems conceivable, reaching all the way to the SK-limit at $r = \infty$. In parallel with the discussion for SK in Sec. IV B, we can at best argue that $\rho = \frac{5}{6}$ is consistent with the trend of the extrapolation. In this plot, a value of $\rho = \frac{3}{4}$ or even that from GBP seems to be ruled out by that trend.

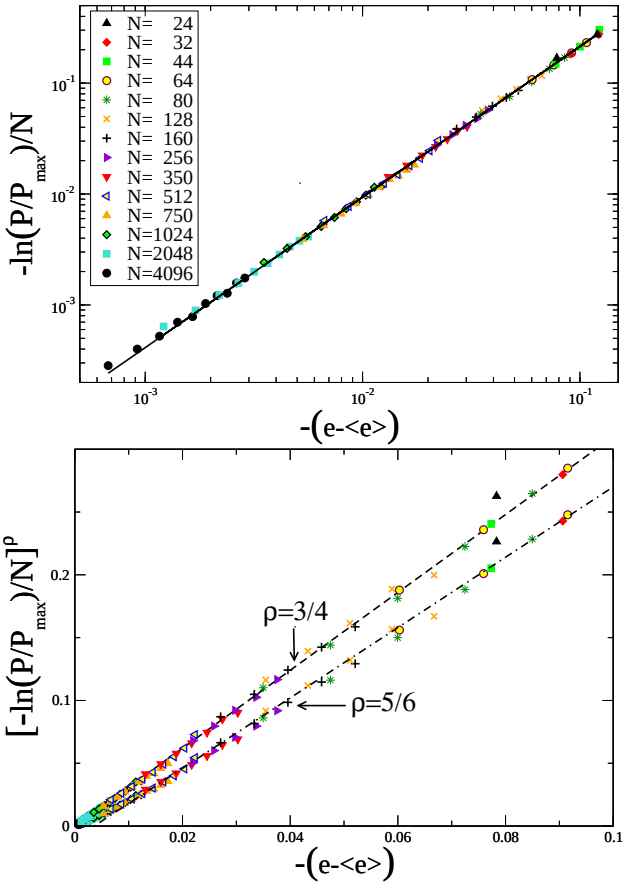

Figure 14: Data collapse on logarithmic scale of all Bethe lattice data for energies *smaller* than the average from Fig. 13. Top, rescaled by an appropriately chosen $P_{\max}$, the data collapses onto a power-law curve, which exhibits scaling over more than a decade. The fit (straight line) gives an exponent of $\rho^{-1} \approx 1.36$. Bottom, the same data is plotted on a linear scale. In this form, $\rho = \frac{3}{4}$ is more consistent with linear scaling (dashed straight lines guide the eye).

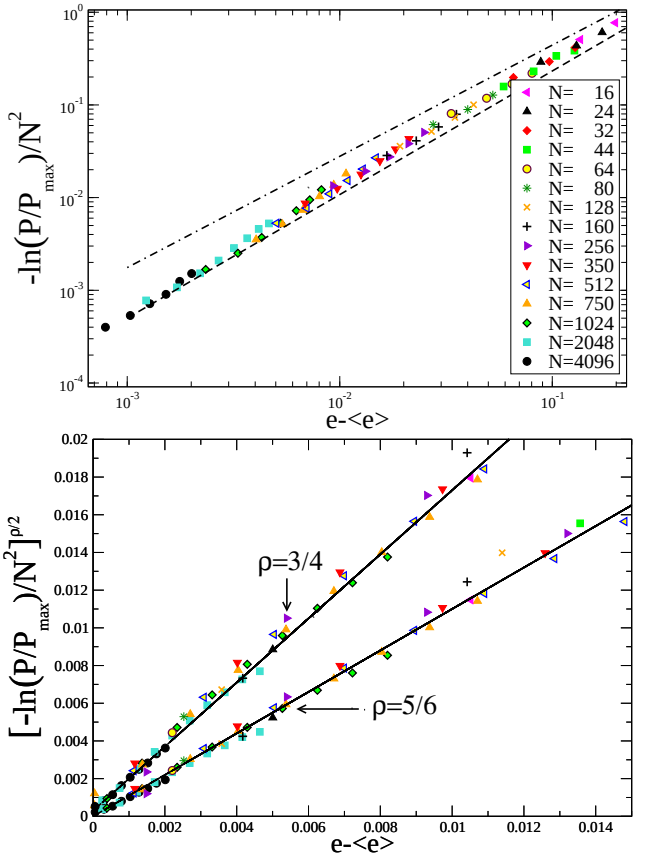

Figure 15: Data collapse on a logarithmic scale (top) of all Bethe lattice data for energies *larger* than the average from Fig. 13. Rescaled by an appropriately chosen $P_{\max}$, the data collapses onto a power-law curve, which exhibits scaling over a decades. Bottom, the same data is plotted on a linear scale. Here, both set of data are somewhat consistent with linear scaling, but the situation is clear than in Fig. 14 (dashed straight lines guide the eye).

C. Extreme Fluctuations

We have attempted a detailed analysis of the tails of the fluctuations for Bethe lattices with the identical approach as conducted in Sec. IV C for SK. The results shown in Figs. 14-15 are indistinguishable from those for SK above, and would also suggest a value closer to $\rho = \frac{3}{4}$ for the Bethe lattice, which seems to contradict the indication provided by the extrapolation of σ in Fig. 8.

VI. SPIN GLASSES ON RANDOM GRAPHS

As a useful reference point to the previous studies, we also include a comparison with a spin glass on sparse, ordinary random graphs of mean degree $C = 2$. It provides an example where fluctuations in the ground states, whether the energy or the cost, appear to converge to a normal distribution. As argued in Sec. II B, it is essential for the case of a fluctuating geometry to focus on the actual cost, i. e. the total absolute weight of the violated bonds, of the ground state. Still, even the PDF for these ground state costs seems asymptotically Gaussian, as has been predicted recently in Ref. [25].

A. Average Ground State Costs

In Tab. VIII, we have listed the average ground state costs and their deviations for a number of system sizes up to $N = 4096$. A large number of instances has been averaged over, even at the largest sizes, since the exact graph reduction methods [39, 40, 57] used for the Bethe lattice above are even more effective here: Even at the largest size, those reductions result in graphs of at most 15% of the original size that need to be optimized with the EO heuristic.

In Fig. 16, we plot the extrapolation of those average ground state costs to the thermodynamic limit. Again,

Table VIII: List of all the data obtained with EO for spin glasses on random graphs of average degree $C = 2$ at system sizes N. Given are the number of instances n_I considered at each N, and the average ground-state cost density $\langle c_0 \rangle_N$ and average standard deviation $\sigma(c_0)$ over these instances.

N	n_I	$\langle e_0 \rangle_N$	$\sigma_N(e_0)$
64	1050000	0.05504(2)	0.01693
128	1050000	0.04994(1)	0.01062
180	1050000	0.04808(1)	0.00846
256	1050000	0.04652(1)	0.00671
360	1050000	0.045296(5)	0.00537
512	1050000	0.044266(4)	0.00429
1024	395722	0.042808(4)	0.00278
2048	668638	0.041883(4)	0.00183
4096	319036	0.041304(4)	0.00123

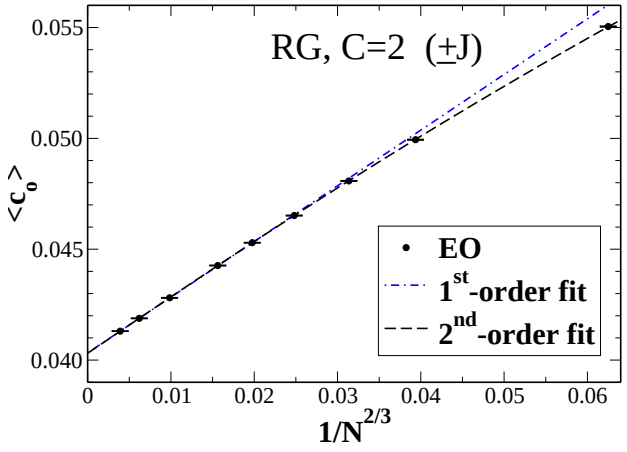

Figure 16: Extrapolation plot of the average ground-state cost densities $\langle c_0 \rangle_N$ for ordinary random graphs of average degree $C = 2$ as a function of the presumed finite-size corrections, $1/N^{\frac{2}{3}}$. As in Fig. 5, the statistical errors indicated are much smaller than symbol sizes. Shown are also a first-order (blue dash-dotted line) and a second-order fit (black dashed line) in powers of $1/N^{\frac{2}{3}}$. For $N \to \infty$, the data extrapolates to $\langle c_0 \rangle_\infty = 0.04030(5)$ at the intercept.

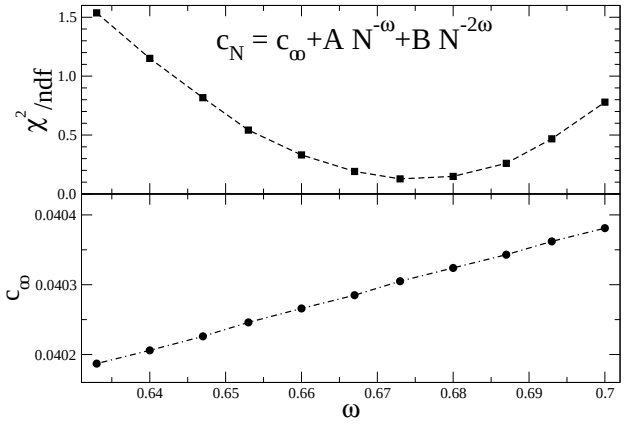

Figure 17: Second-order fit in powers of $N^{-\omega}$ over a range of fixed ω, to the average ground state costs $\langle c_0 \rangle_N$ for spin glasses on random graphs of degree 2 in Tab. VIII. The minimum in χ^2/ndf in the upper plot strongly suggests a pure power series with $\omega = \frac{2}{3}$; such a fit is included in Fig. 16. The lower panel shows the range of extrapolated values in the thermodynamic cost density.

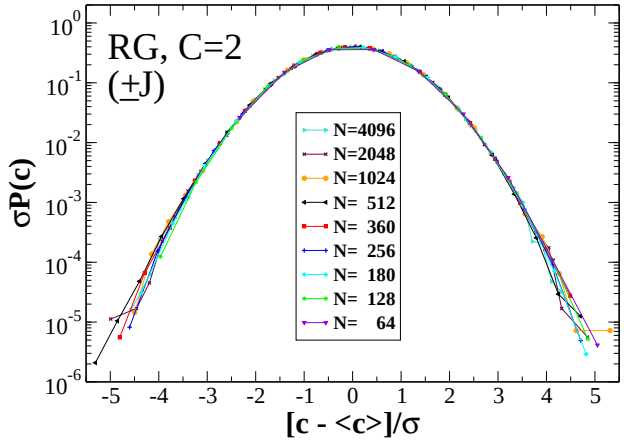

Figure 18: Plot of the probability density functions (PDF) of obtained ground-state cost densities c_0 for the spin glass on an ordinary random graph of average degree 2 in units of the standard deviation σ.

the extrapolation proves most consistent with $N^{-\frac{2}{3}}$ corrections at finite size, although stronger transients are apparent here. In fact, Fig. 17 indicates that finite-size corrections may be a pure power series in $N^{-\frac{2}{3}}$, the first two orders of which are also shown as asymptotic fits in Fig. 16.

B. Ground State Cost Fluctuations

In Fig. 18, we have plotted the PDF for the ground state cost fluctuations. It shows no sign of asymmetry for any size N. Therefore, it is quite surprising that the finite size values obtained for the deviation $\sigma_N(c_0)$ plotted in Fig. 19 and extrapolated in Fig. 20 exhibit a rather slow convergence to a normal width. These results serve as a warning how, even for seemingly trivial fluctuations, the asymptotic behavior might be reached only quite slowly.

VII. THREE-SPIN INTERACTIONS ON BETHE LATTICES

To complement the discussion of glasses with two-spin interactions, and to compare with related work [31, 59], we have also considered spin glasses on Bethe lattices with three-spin interactions, both, with discrete ($\pm J$) and Gaussian bonds, as listed in Tabs. IX and X. This study succeeds in confirming recent observations regarding finite-size corrections to the average ground state en-

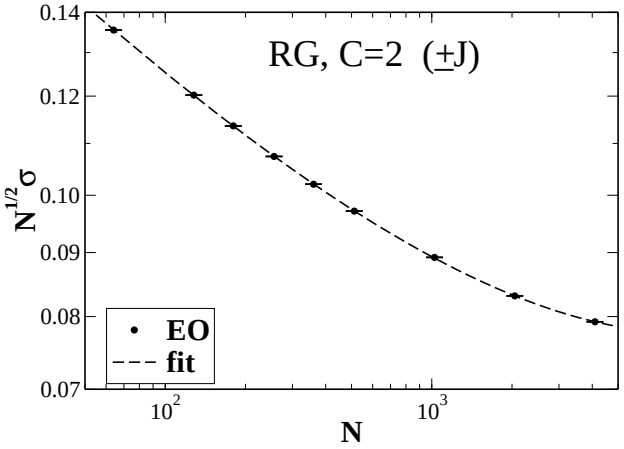

Figure 19: Double-logarithmic plot with system size N of the deviations in the ground state costs, here given as $N^{\frac{1}{2}}\sigma_N(c_0)$ to highlight any difference from Gaussian behavior, for a spin glass on an ordinary random graphs of average degree $C = 2$. The plot is far from flat or linear, suggesting significant corrections to scaling. Expecting asymptotically normal scaling with $\rho = \frac{1}{2}$, we fitted the data with an additional higher-order correction term with $\sim N^{-a}$ (dashed line), as in Eq. (2). The fit determines $a \approx 0.75$.

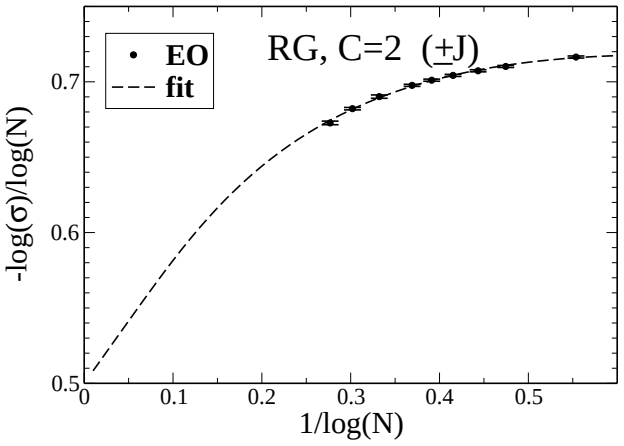

Figure 20: Extrapolation plot of the data for the deviation σ in Tab. VIII according to Eq. (6). A fit is only possible for a fixed $\rho = \frac{1}{2}$.

ergy [31]. But they can merely give a crude picture of deviations within the distribution of those energies. This inadequacy has two origins: First, it proves inherently challenging to determine ground states for instances of this problem with any accuracy already at moderately sized systems. The systems are large enough to predict average energies with reasonable errors, but insufficient for the asymptotic analysis for the deviations. Second, those deviations in their own right appear to be far narrower for this problem than for any of the two-spin models above. In fact, for discrete bonds the grounds states seem to cover only a few states above and below the average, with almost an invariant width, such that the deviations in the density seem to fall with $\sim 1/N$.

Table IX: List of all the data obtained with EO for $p = 3$-spin glasses on Bethe lattices of degree $r = 4$ at system sizes N for discrete bonds. Given are the number of instances n_I considered at each N, and the average ground-state energy density $\langle e_0 \rangle_N$ and standard deviation σ over these instances. The largest system size has unacceptable systematic errors and is ignored in any fit.

N	n_I	$\langle e_0 \rangle_N$	$\sigma_N(e_0)$	N	n_I	$\langle e_0 \rangle_N$	$\sigma_N(e_0)$
15	10000	-1.104(1)	0.0995	51	130000	-1.1760(1)	0.0296
18	100000	-1.1171(3)	0.0834	54	800000	-1.17843(3)	0.0267
24	100000	-1.1406(2)	0.0584	60	25000	-1.1829(2)	0.0242
30	30000	-1.154(3)	0.0500	75	400000	-1.18892(3)	0.0189
33	100000	-1.1576(2)	0.0460	90	35000	-1.1929(1)	0.0157
36	100000	-1.1619(1)	0.0411	120	11000	-1.1973(1)	0.0121
39	100000	-1.1665(1)	0.0365	150	200000	-1.20087(2)	0.0103
45	30000	-1.173(2)	0.0329	180	80000	-1.20264(3)	0.0087
48	800000	-1.17435(3)	0.0319	240	350	-1.1995(4)	0.0067

Table X: List of all the data obtained with EO for $p = 3$-spin glasses on Bethe lattices of degree $r = 4$ at system sizes N for Gaussian bonds. Given are the number of instances n_I considered at each N, and the average ground-state cost density $\langle c_0 \rangle_N$ and standard deviation σ over these instances. The largest system size has unacceptable systematic errors and is ignored in any fit.

N	n_I	$\langle c_0 \rangle_N$	$\sigma_N(c_0)$
33	100000	0.02366(3)	0.00916
39	120000	0.02261(2)	0.00783
51	120000	0.02122(2)	0.00616
66	80000	0.02016(3)	0.00495
99	25000	0.01901(2)	0.00356
144	3500	0.0193(1)	0.00274

A somewhat wider distribution is observed for Gaussian bonds, which provides for a smoother appearance for the PDF at all system sizes compared to the discrete case. Any skewness can only be observed when plotted for ground state *cost* fluctuations; energy fluctuations would always be normal, originating from the random fluctuations in the total bond-weight themselves, as described in Sec. II B. Surprisingly, these cost fluctuations skew exactly in the opposite direction from any previous studied PDF, such as those above. Although the deviations σ extracted from those PDFs indeed seem inconsistent with $1/N$ scaling, the system sizes attained in this study are rather small, $N \leq 100$, and asymptotic behavior may not have been reached in this study.

A. Ground State Energy

In Figs. 21-22, we extrapolate the obtained average ground state energies (for discrete bonds) or costs (for

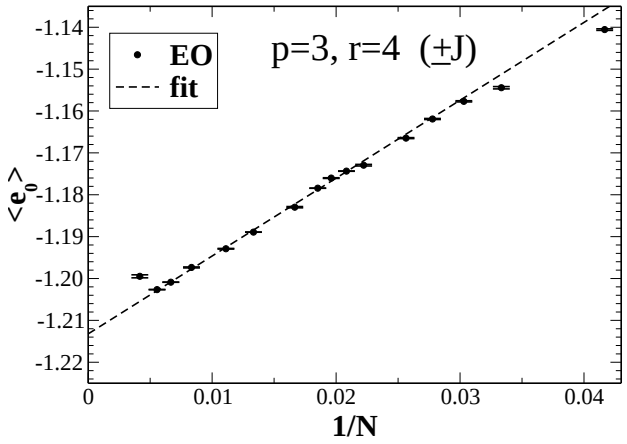

Figure 21: Extrapolation plot of the average ground-state energy densities $\langle e_0 \rangle_N$ for a spin glass with discrete bonds in which $p = 3$ spins mutually interact on a Bethe lattices of degree $r = 4$, as a function of the presumed finite-size corrections, $1/N$.

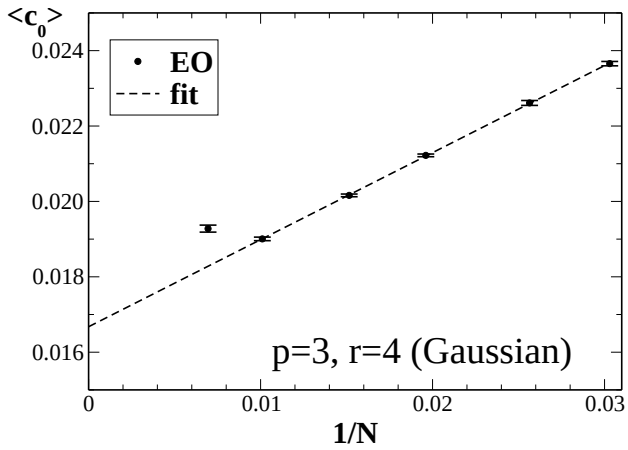

Figure 22: Extrapolation plot of the average ground-state cost densities $\langle e_0 \rangle_N$ for a Gaussian spin glass with three-spin interactions on a Bethe lattices of degree $r = 4$, as a function of the presumed finite-size corrections, $1/N$.

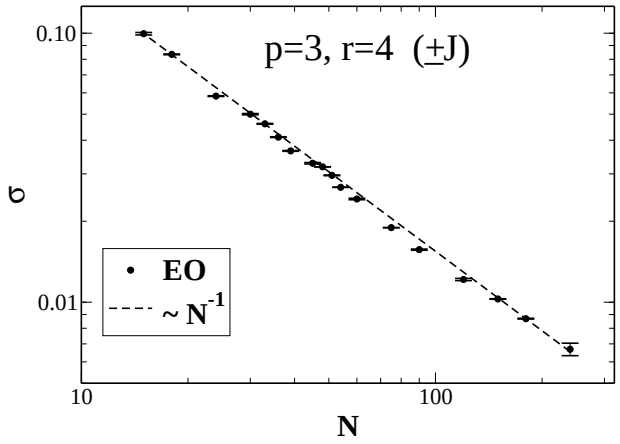

Figure 23: Log-log-plot of the deviations σ in the ground state energy fluctuations of a $p = 3$ spin glass on Bethe lattices of degree $r = 4$ as a function of system size N. The data is very difficult to fit, and we only provide the dashed line $\sim 1/N$ as a guide to the eye.

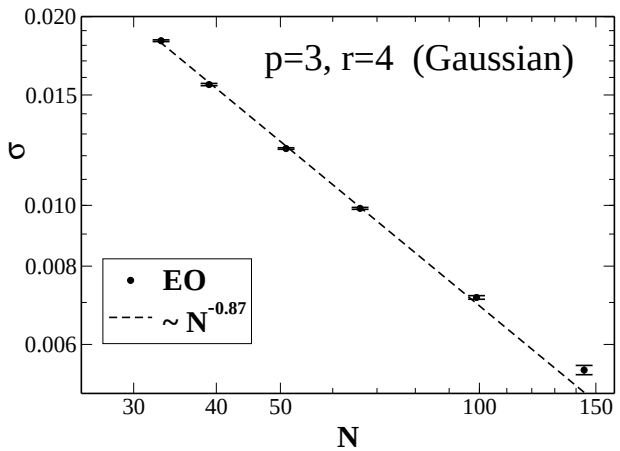

Figure 24: Log-log-plot of the deviations σ in the ground state energy fluctuations for a $p = 3$-spin glass on Bethe lattices of degree $r = 4$ as a function of system size N, here for Gaussian bonds. As for the plot for discrete bonds in Fig. 23, this data is also difficult to fit, and there is a visible trend to even lower values in the exponent then 0.87 found by only fitting to sizes $N \leq 100$ (dashed line).

Gaussian bonds) in Tabs. IX and X. In both cases, finite size corrections appear to decay with volume corrections, like $1/N$, stronger than in any of the $p = 2$-spin models above. Hence, even though the system sizes are small, quite reasonable extrapolations are achieved. In the discrete case in Fig. 21 there appears to be significant structure in the transients. By reproducing the exact ground states for a sample of those instances up to size $N = 51$ with exact (branch-and-bound) algorithms, we have verified that these are not due to systematic errors in the optimization heuristic, as 100% agreement was achieved for each instance. Rather, we expect that those effects are due to the constraints in the formation of 4-regular hypergraphs at small N in combination with the discrete set of bonds available. Correspondingly, the Gaussian data is free of any such structure, and thus extrapolates with comparable accuracy despite the overall smaller system sizes used.

For $N \to \infty$, the discrete data in Fig. 21 extrapolates to $\langle e_0 \rangle_\infty = -1.213(2)$ at the intercept, slightly above the one-step replica symmetry-breaking (RSB) prediction [59], as would be expected for the true ground state at full RSB. With bonds drawn from a Gaussian distribution, we instead plot the actual cost of violated bonds. It is difficult to obtain good minima already at $N \approx 100$, such that we can only extrapolate data for smaller N. For $N \to \infty$, the extrapolation yields a cost of $\langle c_0 \rangle_\infty = 0.0167(4)$ at the intercept. Since average cost and energy density for Gaussian bonds are related via

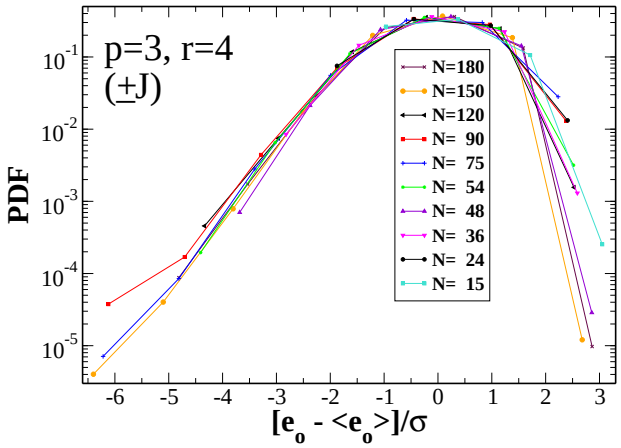

Figure 25: Plot of the probability density functions (PDF) of obtained ground-state energy densities e_0, in units of the standard deviation σ, for the $p = 3$-spin glass with discrete bonds on an $r = 4$-regular random graph. The rugged appearance of the data is due to the discreteness of the bonds and the fact that only a very narrow set of energy values around the mean are taken on.

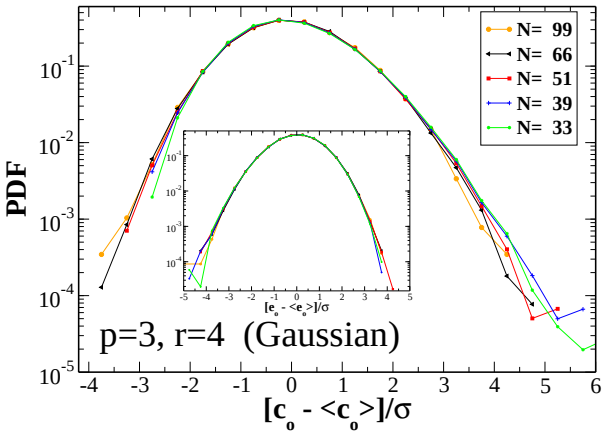

Figure 26: Plot of the probability density functions (PDF) of obtained ground-state *cost* densities c_0, in units of the standard deviation σ, for the $p = 3$ spin glass with Gaussian bonds on an $r = 4$-regular random graph. The data is skewed with a sharp cut-off for costs less than the average and a long tail for larger cost, exactly opposite to any previous PDF for energy fluctuations. The inset shows the same data plotted as energy fluctuation PDF, which are purely normal distributed.

Eq. (7), we obtain with $\langle |J| \rangle = \sqrt{\frac{2}{\pi}}$, $r = 4$, and $p = 3$ that $\langle e_0 \rangle = -1.030(1)$.

B. Ground State Fluctuations

In light of the limited ability to produce ground states at larger system sizes, any prediction for the fluctuation exponent ρ is poor. Furthermore, extreme fluctuations are difficult to attain, since the width is rather narrow. Yet, for discrete bonds the data plotted for σ in Fig. 23 is quite consistent with $1/N$-decay, i. e. $\rho = 1$. But there does not seem to be a clear trend towards asymptotic scaling in the case of Gaussian bonds shown in Fig. 24. If anything, the data appears to exhibit upward curvature, away from an $1/N$ scaling regime, indicating that ρ in this case may be even lower than the fitted value of ≈ 0.87. Such a discrepancy between discrete and Gaussian bonds on Bethe lattices was also noted for the $p = 2$-spin model [32].

With the rapid decay of the width for discrete bonds, it is not surprising that the PDF for its energy fluctuations has a somewhat rugged appearance: only few, discrete energy values can be taken on left or right of the mean. As shown in Fig. 25, the PDF otherwise skews similarly to all previous cases. It comes as a surprise then, that the corresponding PDF for Gaussian bonds in Fig. 26 skews exactly in the opposite direction. Although it is plotted for the cost fluctuations instead – the energy fluctuations in the inset are purely normal –, this does not explain the difference in the skewness, since cost and energy are linearly related [as in Eq. (7)]. Lower cost correlates with lower energy and vice versa. We speculate that the skewness here has a rather trivial origin: As indicated by the very low average ground state cost per spin, $\langle c_0 \rangle_\infty = 0.0167(4)$ (about 1/4 of that for discrete bonds), below-average-cost instances may be hard to find due to the proximity of entirely cost-free, "perfect" solutions (although we have not actually generated a single solvable instance during our study). On the other hand, higher-cost instances are likely produced by the addition of isolated "defects" in the quenched bonds that can not be gauge-transformed away as easily as in SK [55] (or probably other problems), where many such frustrated plaquettes overlap. The smooth and well-converged appearance of the PDF in Fig. 26 may provide some confidence that the lack of scaling in the respective deviations σ in Fig. 24 is not due to a systematic error in the sampling. It is the nature of heuristic optimization that any bias at large system sizes (larger than can be verified by exact methods) can never be exclude. But as the examples in the previous sections demonstrate, strong competition between correction terms may be equally well a cause in precluding asymptotic scaling.

We can address the puzzling skewness for the Gaussian case further by comparing with previous results with Gaussian bonds on $p = 2$-spin glasses on Bethe lattices. While we have experienced this case already for discrete bonds at $r = 3$ above in Sec. V without any qualitative difference in behavior compared to the SK model, its Gaussian version presents a very odd pattern. In Ref. [32] we have already remarked on the unusual finite-size corrections to the thermodynamic average ground state cost or energy and the confusing trend that already beset the cost deviations $\sigma(c_0)$. We therefore missed the even more surprising evolution with r and N of the skewness in the corresponding PDFs. Aside from some finite-size effects, all PDFs for the energies are approximately normal dis-

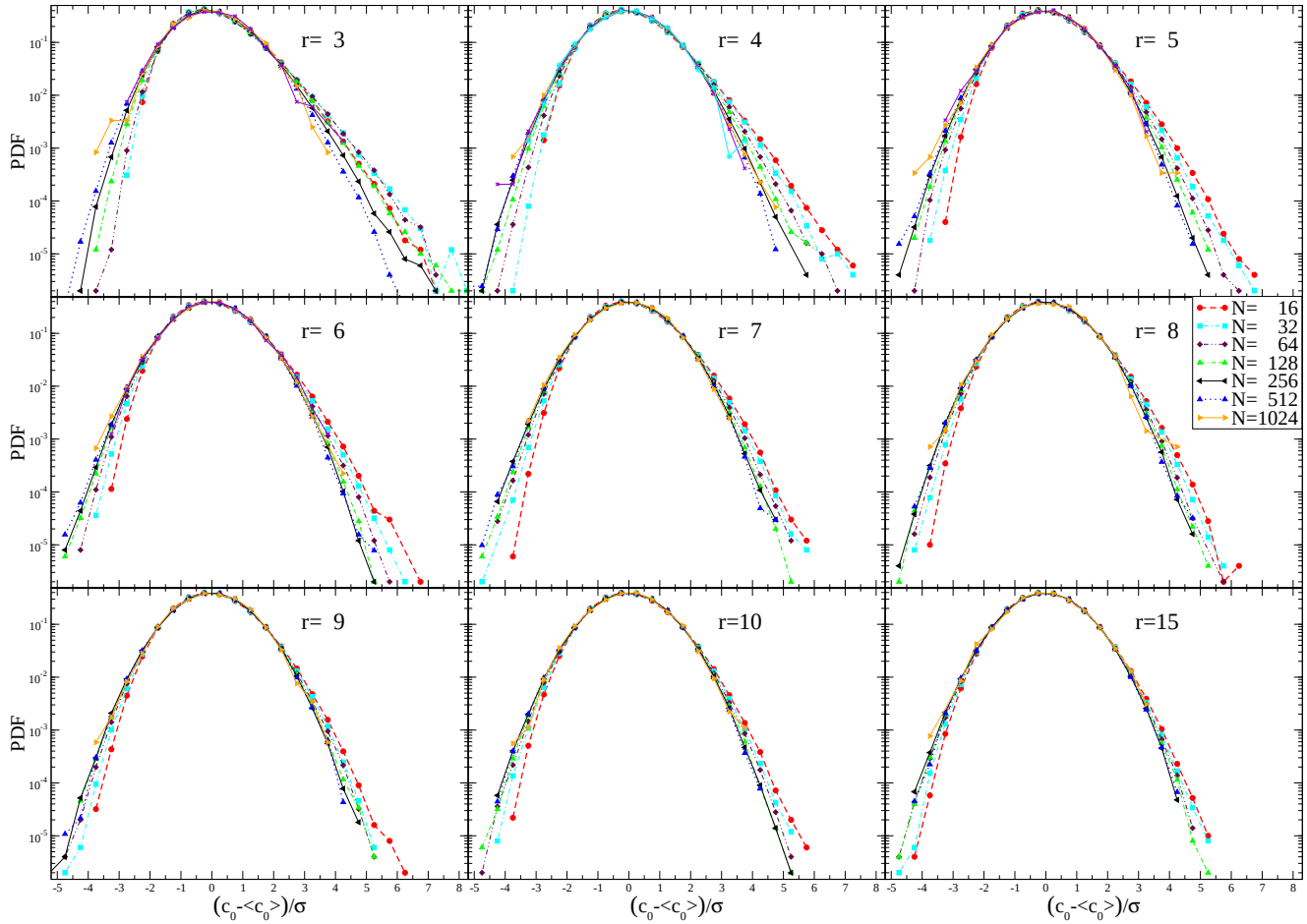

Figure 27: Plot of the PDFs for the fluctuations of the ground state costs per spin for a $p = 2$-spin glass with a Gaussian bond distribution on Bethe lattices of degree $r = 3, 4, \ldots, 10, 15$. For smaller r and sizes N, the PDFs are right-skewed, just as in Fig. 26, but especially for larger r those PDFs appear to approach a normal distribution for large sizes N.

tributions. But the PDFs for cost fluctuations shown in Fig. 27 range from those strongly skewed, comparable to Fig. 26, for small r to those with only mild skewness at larger r. For all cases, but most drastically for larger r, increasing system size N symmetrizes the PDFs towards an apparent normal shape. Note that for the SK limit $r \to \infty$, these distribution should approach a normal form for the cost. While energy fluctuations should become the non-trivial PDF in the SK limit, $r = 15$ is apparently not large enough for this effect to be discernible.

VIII. CONCLUSIONS

To elucidate the origin of the unusual ground state deviations observed in the SK model, we have parsed over a range of different spin glass and combinatorial models in an effort to provide context for any typical or atypical properties. The clearest picture emerges from graph-bipartitioning (GBP) on Bethe lattices, corresponding to a ferromagnetic system held at zero magnetization. The scaling exponent ρ for each degree r of the network possesses a convincing extrapolation, but to values unlike those proposed for SK [20–25], suggesting a very different origin for the fluctuations in GBP. At best, they come closest to the value of $\rho = \frac{4}{5}$ recently found for the m-vector spin glass [27]. The situation for the SK is less clear, apparently due to very strong higher-order corrections in the finite-size behavior. Although far from a scaling with the theoretically favored value of such a behavior for the SK becomes plausible with very close $1/N$ corrections, a scenario further supported by the Bethe lattice spin glass at degree $r = 3$ (with discrete bonds) exhibiting very similar behavior but inherently closer to $\rho = \frac{5}{6}$. As the example of the vector model demonstrates, entirely distinct values are conceivable for any of these models, but since in the limit $r \to \infty$ the Bethe lattices approaches SK, such a distinction seems implausible. A look deep into the tails for SK and the Bethe lattices, for which extensive results have been generated, would suggest that the scaling of the deviations σ with the exponent ρ that is dominated by near-typical fluctu-

ations may be disconnected from the extremely atypical fluctuations deep in the tails, which is more consistent with $\frac{3}{4}$-scaling for both models. But despite the massive amount of data obtained here, any true asymptotic scaling for the tails may still be elusive.

The situation might be simpler for models in which more than two spins interact. For instance, we find for a $p = 3$-spin glass model with discrete bonds on a $r = 4$-regular Bethe lattices that fluctuations scale about with $1/N$, i. e. $\rho = 1$, which would already attain the result for the REM ($p \to \infty$) [14] in Ref. [23]. On the other hand, the same model with Gaussian bonds demonstrates the fragility of the phenomenon: energy-fluctuations get overwhelmed by trivial (normal) fluctuations in the continuous bond weights, while the more pertinent cost-fluctuations are skewed exactly in the opposite direction from those from SK, or even those on the same graph with discrete bonds. A same effect is found for $p = 2$ on Bethe lattices at low r. In summary, the large variation in behaviors of fluctuations not only between models, but even within models for different bond distributions, hints at the strong dependence on minute details of the underlying graph geometry and variability in bond weights. Either can impact whether and how frustrated plaquettes correlate to ease the cost when an instance possesses more or less of those than the average.

Acknowledgments

I would like to thank F. Ricci-Tersenghi for numerous helpful correspondences during the preparation of this manuscript, and I gratefully acknowledge support from the Fulbright Kommission and from the U. S. National Science Foundation through grant number DMR-0812204.

[1] S. F. Edwards and P. W. Anderson, J. Phys. F **5**, 965 (1975).
[2] M. Mézard, G. Parisi, and M. A. Virasoro, *Spin glass theory and beyond* (World Scientific, Singapore, 1987).
[3] M. Mézard and A. Montanari, *Constraint Satisfaction Networks in Physics and Computation* (Oxford University Press, Oxford, 2006).
[4] H. Nishimori, *Statistical Physics of Spin Glasses and Information Processing* (Oxford University, Oxford, 2001).
[5] J. J. Hopfield, PNAS **79**, 2554 (1982).
[6] E. Schneidman, M. J. Berry, R. Segev, and W. Bialek, Nature **440**, 1007 (2006).
[7] D. Sherrington and S. Kirkpatrick, Phys. Rev. Lett. **35**, 1792 (1975).
[8] M. Palassini, cond-mat/0307713v1.
[9] J.-P. Bouchaud, F. Krzakala, and O. C. Martin, Phys. Rev. B **68**, 224404 (2003).
[10] A. Andreanov, F. Barbieri, and O. C. Martin, Eur. Phys. J. B **41**, 365 (2004).
[11] S. Boettcher, Eur. Phys. J. B **46**, 501 (2005).
[12] M. Palassini, J. Stat. Mech. P10005 (2008).
[13] J.-P. Bouchaud and M. Mézard, J. Phys. A: Math. Gen. **30**, 7997 (1997).
[14] B. Derrida, Phys. Rev. Lett. **45**, 79 (1980).
[15] M. Körner, H. G. Katzgraber, and A. K. Hartmann, J. Stat. Mech. P04005 (2006).
[16] C. Monthus and T. Garel, J. Stat. Mech. P02023 (2010).
[17] T. Aspelmeier, J. Stat. Mech., P04018 (2008).
[18] T. Aspelmeier, Physical Review Letters **100**, 117205 (2008.
[19] T. Aspelmeier, M. A. Moore, and A. P. Young, Phys. Rev. Lett. **90**, 127202 (2003).
[20] A. Crisanti, G. Paladin, and H.-J. S. A. Vulpiani, J. Phys. I **2**, 1325 (1992).
[21] T. Aspelmeier, A. Billoire, E. Marinari, and M. A. Moore, Journal of Physics A: Mathematical and Theoretical **41**, (2008).
[22] G. Parisi and T. Rizzo, Phys. Rev. Lett. **101**, 117205 (2008).
[23] G. Parisi and T. Rizzo, Phys. Rev. B **79**, 134205 (2009).
[24] G. Parisi and T. Rizzo, arxiv.org:0901.1100.
[25] G. Parisi and T. Rizzo, J. Phys. A: Math. Theor. **43**, 045001 (2010).
[26] J. Wehr and M. Aizenman, J. Stat. Phys. **60**, 287 (1990).
[27] T. Aspelmeier and A. Braun, arxiv.org:1001.0893.
[28] S. Boettcher, Phys. Rev. Lett. **95**, 197205 (2005).
[29] S. Boettcher, Euro. Phys. J. B **31**, 29 (2003).
[30] S. Boettcher, Phys. Rev. B **67**, R060403 (2003).
[31] T. Nakajima and K. Hukushima, Phys. Rev. E **80**, 011103 (2009).
[32] S. Boettcher, Euro. Phys. J. B **74** (2010), to appear.
[33] L. Zdeborova and S. Boettcher, J. Stat. Mech. P02020 (2010).
[34] S. Boettcher and A. G. Percus, Artificial Intelligence **119**, 275 (2000).
[35] S. Boettcher and A. G. Percus, Phys. Rev. Lett. **86**, 5211 (2001).
[36] A. Hartmann and H. Rieger, eds., *New Optimization Algorithms in Physics* (Wiley-VCH, Berlin, 2004).
[37] H. Bauke and S. Mertens, Phys. Rev. E **70**, 025102(R) (2004).
[38] A. G. Percus, G. Istrate, B. Gonçalves, R. Z. Sumi, and S. Boettcher, Journal of Mathematical Physics **49**, 125219 (2008).
[39] S. Boettcher, Euro. Phys. J. B **38**, 83 (2004).
[40] S. Boettcher, Europhys. Lett. **67**, 453 (2004).
[41] M. R. Garey and D. S. Johnson, *Computers and Intractability: A Guide to the Theory of NP-Completeness* (W. H. Freeman, New York, 1979).
[42] C. J. Alpert and A. B. Kahng, Integration: The VLSI Journal **19**, 1 (1995).
[43] B. A. Hendrickson and R. Leland, in *Proceedings of Supercomputing '95* (1995).
[44] S. Boettcher, Computing in Science and Engineering **2**, 75 (2000).
[45] S. Boettcher, J. Phys. A: Math. Gen. **32**, 5201 (1999).
[46] S. Boettcher and A. G. Percus, Phys. Rev. E **64**, 026114 (2001).

[47] J. R. Banavar, D. Sherrington, and N. Sourlas, J. Phys. A: Math. Gen **20**, L1 (1987).
[48] M. Mezard and G. Parisi, Europhys. Lett. **3**, 1067 (1987).
[49] K. Y. M. Wong and D. Sherrington, J. Phys. A: Math. Gen. **20**, L793 (1987).
[50] K. Y. M. Wong, D. Sherrington, P. Mottishaw, R. Dewar, and C. D. Dominicis, J. Phys. A: Math. Gen. **21**, L99 (1988).
[51] R. Oppermann, M. J. Schmidt, and D. Sherrington, Phys. Rev. Lett. **98**, 127201 (2007).
[52] G. Parisi, F. Ritort, and F. Slanina, J. Phys. A **26**, 247 (1993).
[53] G. Parisi, F. Ritort, and F. Slanina, J. Phys. A **26**, 3775 (1993).
[54] H. G. Katzgraber, M. Körner, F. Liers, M. Jünger, and A. K. Hartmann, Phys. Rev. B **72**, 094421 (2005).
[55] S. Boettcher and T. M. Kott, Phys. Rev. B **72**, 212408 (2005).
[56] D. S. Dean and S. N. Majumdar, Phys. Rev. Lett. **97**, 160201 (2006).
[57] S. Boettcher and J. Davidheiser, Phys. Rev. B **77**, 214432 (2008).
[58] M. Mezard and G. Parisi, J. Stat. Phys. **111**, 1 (2003).
[59] S. Franz, M. Leone, F. Ricci-Tersenghi, and R. Zecchina, Phys. Rev. Lett. **87**, 127209 (2001).
[60] A sample code of this implementation of EO for SK can be found at http://www.physics.emory.edu/ faculty/boettcher/Research/EO_demo/demoSK.c.